# SOIL COMPACTION

## EFFECTS ON SOIL HYDRAULIC PROPERTIES
## AND
## PREFERENTIAL WATER FLOW

Mona Mossadeghi Björklund

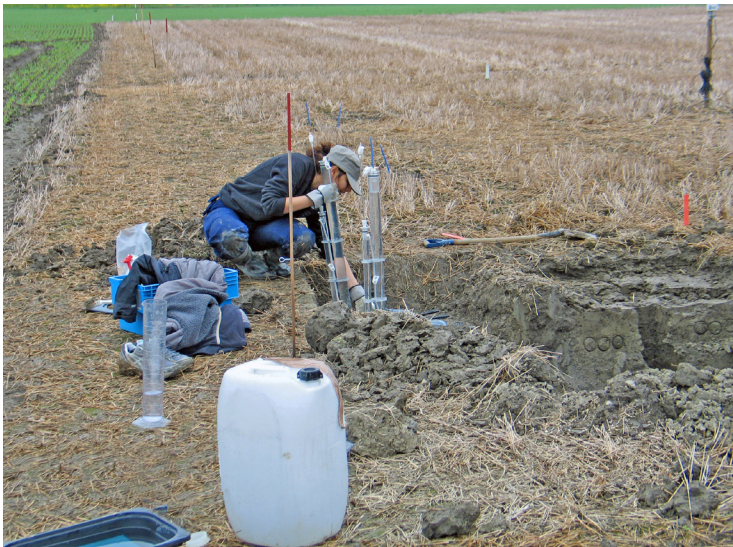# SOIL COMPACTION

## EFFECTS ON SOIL HYDRAULIC PROPERTIES
## AND
## PREFERENTIAL WATER FLOW

Mona Mossadeghi Björklund

*Swedish University of Agricultural Sciences*
*Department of Soil and Environment*
*Uppsala*

**s l u**

**SWEDISH UNIVERSITY
OF AGRICULTURAL
SCIENCES**

Licentiate thesis
Swedish University of Agricultural Sciences
Uppsala 2020

Cover: Jokioinen, POSEIDON-NORDIC project
    (photo: A, Simojoki)

# Abstract

Soil compaction caused by passage of agricultural machinery over the surface is an issue in many agricultural soils with a high clay content. Compaction is known to modify soil pore structure and soil hydraulic properties, but can also affect the occurrence of preferential flow. Water flow through preferential flow pathways can facilitate transport of fertilisers, pesticides and contaminants to groundwater, creating harmful environmental problems. In two complementary studies, this thesis examined soil hydraulic properties and preferential water flow on soil cores sampled in the field and quantified flow patterns *in situ* at two sites approximately 300 m apart in central Sweden. One year after compaction of field plots, X-ray computed tomography (CT) imaging was used to visualise and quantify soil pore structures in soil columns taken from the subsoil (30-50 cm depth). Degree of preferential water flow and transport were derived from non-reactive tracer breakthrough curves. Dye tracing experiments were performed in the field and different soil mechanical and hydraulic properties were measured to help explain the dye patterns.

Contrasting effects of wheel traffic were observed at the two neighbouring sites. Thus, even quite small differences in initial soil and site conditions can significantly influence the extent to which applied compaction stresses affect the connectivity of structural pore space in soil and, consequently, water flow patterns. These results contradict previous findings of an increase in preferential flow following soil compaction. This discrepancy in results was analysed with the help of a conceptual model, which suggested that preferential flow is greatest at some intermediate level of compaction at which macropore continuity is still maintained, despite reductions in macroporosity. The model also illustrated how compaction, and subsequent recovery from compaction, might affect susceptibility to preferential flow and surface runoff. To prevent subsoil compaction, it is important to consider soil conditions at the time of trafficking, which can significantly influence the effect of compaction on soil pore connectivity and associated water flow.

*Keywords:* Subsoil compaction, air permeability, breakthrough curve, CT-imaging, penetration resistance, saturated hydraulic conductivity, dye tracing, macroporosity, soil pore structure, water flow

*Author's address:* Mona Mossadeghi Björklund, Department of Soil and Environment, SLU, P.O. Box 7014, 750 07 Uppsala, Sweden
*E-mail:* mona.mossadeghi@slu.se

# Dedication

To my sons, Yosef and Yones.

*Education is not the learning of facts, but the training of the mind to think.*
   Albert Einstein

# Contents

**Acknowledgements** 47

# List of Publications

This thesis is based on the work contained in the following papers, referred to by Roman numerals in the text:

I   Mossadeghi-Björklund, M., Arvidsson, J., Keller ,T., Koestel, J., Lamandé, M., Larsbo, M. & Jarvis, N. 2016. Effects of subsoil compaction on hydraulic properties and preferential flow in a Swedish clay soil. *Soil & Tillage Research* 156: 91-98.

II  Mossadeghi-Björklund, M., Jarvis, N., Larsbo, M., Forkman, J. & Keller, T. 2019. Effects of compaction on soil hydraulic properties, penetration resistance and water flow patterns at the soil profile scale. *Soil Use and Management* 35(3): 367-377.

Papers I-II are reproduced with the permission of the publishers.

The contribution of Mona Mossadeghi-Björklund to the papers included in this thesis was as follows:

I    Performed the field and laboratory work and carried out data analysis with supervision from NJ, JA, TK, ML and JK. Mathieu Lamandé performed the CT image analyses. Designed the paper layout and did most of the writing.

II   Performed the field and laboratory work and carried out data analysis with supervision from NJ, TK, ML and JK. Designed the paper layout and did most of the writing.

# Abbreviations

| Symbol | Definition |
| --- | --- |
| BTC | Breakthrough curve |
| $K_s$ | Saturated hydraulic conductivity |
| $K_a$ | Air permeability |
| $t_{0.05}$ | 5% arrival time |
| CT | Computed tomography |

# 1 Introduction

## 1.1 Soil compaction

Soil compaction in a strict sense is the process by which bulk density increases and soil porosity decreases. Compaction may be caused by passage of agricultural machinery over the field and typically not only reduces pore volume, but also modifies pore connectivity and continuity and pore size distribution (Servadio *et al*., 2001). Previous studies suggest that compaction reduces the saturated and near-saturated hydraulic conductivity of soil (Arvidsson, 1997; Schwen *et al*., 2011) and increases the risk of surface runoff (Lipiec & Hatano, 2003). Compaction may also increase the probability of preferential flow in any remaining macropores (Kulli *et al*., 2003) or those that regenerate after compaction (Jarvis, 2007). This can facilitate transport of fertilisers, pesticides and pollutants to receiving water bodies and groundwater resources.

There is a difference between topsoil and subsoil compaction. Topsoil compaction refers to compaction within tillage depth (0-0.3 m) and is caused primarily by pressure applied to the soil surface. Freeze-thaw and wetting-drying cycles can help reverse topsoil compaction. The effects of topsoil compaction may also be partly reversed by mouldboard ploughing (Arvidsson & Håkansson, 1996), whereas the effects of subsoil compaction may be more persistent (Etana & Håkansson, 1994). Due to its persistence, subsoil compaction is a major concern for agricultural soils. Some field operations, such as deep subsoiling, can alleviate subsoil compaction, but the result is not always worth the costs (Chamen *et al*., 2015). Therefore, efforts should be made to minimise soil compaction due to its harmful effects on soil pores, and subsequent negative consequences for plant root growth and enhanced runoff and leaching of fertilisers and pesticides to groundwater (Kim *et al*., 2010).

## 1.2 Macropores and preferential flow

Macropores are large, continuous structural pores in soil and include shrinkage cracks, tillage fractures, root channels and soil fauna burrows. It has been suggested that pores larger than about 0.3-0.5 mm diameter, which are equivalent (assuming cylindrical pore shape) to pores that empty at water pressures of -10 to -6 cm, can be classified as macropores (Jarvis, 2007). They are important because they largely govern transport functions. Preferential flow refers to non-equilibrium flow where water and solutes move rapidly through the macropores and only interact with the soil matrix to a limited extent. Because of rapid water movement, preferential flow can lead to faster solute transport and affect groundwater quality by fertiliser and pesticide leaching (Vanclooster *et al.*, 1995; Goulding *et al.*, 2000).

In general, two conditions must be met for macropores to contribute to preferential flow. First, the macropore must be partly or completely filled with water and, second, the macropore must extend continuously over a significant portion of the porous medium (Hendrickx *et al.*, 2001). A common example of preferential flow at pore scale is flow through earthworm burrows or root channels when a section of the soil matrix reaches saturation or at least is close to saturation. Water and chemicals can bypass the topsoil by travelling in such channels, and pollutants and pesticides can potentially contaminate shallow groundwater resources.

Although preferential flow is typically associated with flow through macropores, it can also occur at other scales, referred to as Darcian scale and areal scale (Hendrickx *et al.*, 2001). At the Darcian scale, preferential flow may occur in homogeneous soils with no pronounced macropore structure, *e.g.* in soils where coarse-textured layers are overlain by less permeable layers or in soils with water-repellent zones. At the areal scale, surface depressions and discontinuous layers with lower or higher permeability can cause preferential flow. In this thesis work, the focus was on preferential flow at the pore to profile scale, *i.e.* predominantly preferential flow through macropores.

## 1.3 Methods to quantify the occurrence of preferential flow

Preferential flow is difficult to measure and quantify. One important reason for the limited progress to date in quantification of preferential flow is the difficulty in quantifying important pore system characteristics that control water flow and solute transport. Thus, evidence of preferential flow is often indirectly inferred from unexpectedly early water and chemical breakthrough or from unexpectedly deep water and chemical migration in soil. Today, there are many methods available to quantify macropore networks in soil, each with their own advantages

and disadvantages (Allaire *et al*., 2009). Dye tracer experiments and X-ray computed tomography (CT) techniques are the most commonly used approaches to characterise preferential flow through macropores. Dye tracer experiments provide qualitative pictures to illustrate the flow pathways in soil (Alaoui & Goetz, 2008) and dye tracing is generally a reliable technique for visualisation, identification and quantification of water flow pathways in structured soils (Janssen & Lennartz, 2008). Direct evidence of the presence of preferential flow can be obtained from dye tracer patterns (Hendrickx & Flury, 2001). However, dye tracer tests only provide information in two dimensions. They are also relatively work-intensive, requiring excavation of soil pits and preparation of soil profile walls.

In contrast, X-ray CT imaging is an effective non-destructive scanning method that can visualise and quantify soil pore structures in three dimensions (Kim *et al*., 2010; Lamandé *et al*., 2013; Larsbo *et al*., 2014). A CT image is a three-dimensional image of the inside of an object constructed from a large series of two-dimensional X-ray images taken around a single axis of rotation. Petrovic *et al*. (1982) were the first to apply CT imaging in soil science, with the aim of determining soil bulk density. Since their work, the use of CT imaging in soil science studies has increased greatly. The results have considerably improved understanding of how soil structure and pore connectivity influence water movement, particularly in soils where preferential flow is prevalent (Mooney, 2002). Computed tomography imaging can also be a very useful approach in studies targeting characterisation of soil pore modification after compaction (Pires, 2011). However, while CT imaging techniques have great potential, they also have severe drawbacks in terms of accessibility, resolution and artefacts (Mooney, 2002). For example, CT imaging is restricted to analysis of "isolated" soil cores, whereas dye tracing allows investigation of water flow within a whole soil profile (Wildenschild & Sheppard, 2013). Thus, sample size is one limitation of the technique. Therefore, in this thesis, both CT images and dye tracing patterns were used to gain a better understanding of the flow and transport properties in soil after compaction.

The degree of preferential flow can also be quantified in intact soil columns in breakthrough curve (BTC) experiments. In this method, a solution containing the chemical of interest is applied to one end of the soil column and its concentration is measured in the effluent at the other end of the column, under steady water flow. The relationship between the relative solute concentration in the effluent and time elapsed or amount of water passing through the soil column is called the breakthrough curve. The shape of the breakthrough curve is then analysed to study the function of the pore system in the transport process. From the shape of breakthrough curves, useful information such as the 5% arrival time

($t_{0.05}$), *i.e.* the time, relative to the average arrival time, for 5% of the applied tracer mass to arrive at the bottom of the sample, can be obtained. The $t_{0.05}$ value obtained can be used to deduce the presence of preferential flow (Koestel *et al.*, 2011). It has been identified as a robust indicator of preferential transport, with smaller $t_{0.05}$ values indicating stronger preferential flow (Ghafoor *et al.*, 2013; Knudby & Carrera, 2005; Koestel *et al.*, 2011, 2012). In a study carried out on 733 tracer BTC experiments by Koestel *et al.* (2012), it was suggested that $t_{0.05}$ >0.5 indicates absence of preferential flow, while values <0.22 indicate strong preferential flow.

## 1.4   Compaction effects on the pore system and preferential flow

It is generally suggested that compaction results in a massive soil structure, through homogenisation of the pore system and creation of smaller pores (Servadio *et al.*, 2001). The pore fractions most affected by compaction include macropores or coarse mesopores (Alaoui *et al.*, 2011; Cassaro *et al.*, 2011), which are vitally important for soil aeration and water transport. For example, Lipiec and Håkansson (2000) found that an increase in the number of vehicle-passes from zero to eight decreased macroporosity from 13.4% to 5.6%. Compaction not only modifies the pore volume, but also alters the connectivity and continuity of pores (Alaoui *et al.*, 2011). Changes in the characteristics and geometry of structural pore networks following compaction can significantly influence the risk of rapid preferential solute transport in soil macropores (Hendrickx & Flury, 2001; Jarvis, 2007). As compaction mainly disrupts or destroys the larger pores in soil, it can be expected to reduce the strength of preferential flow, *e.g.* Heitman *et al.* (2007) observed slower breakthrough of non-reactive solute in compacted plots. On the other hand, some studies report strong preferential flow following compaction in macropores remaining after compaction, or macropores regenerated later due to physical or biological processes (Alaoui & Goetz, 2008; Kulli *et al.*, 2003).

# 2 Thesis work

The aim of this thesis was to determine the effects of compaction on soil hydraulic properties and identify how this affects preferential flow in soil. To achieve this objective, two complementary studies (Papers I and II) were carried out at the same two experimental sites. Paper I focused on soil hydraulic properties and preferential water flow in soil columns sampled in the field, while Paper II involved *in situ* quantification of flow patterns. Both studies combined field and laboratory data from the same sites, to gain a better understanding of compaction effects on preferential flow.

## 2.1 Paper I: Compaction effects on preferential flow

Paper I examined the effects of compaction on preferential water flow in soil columns (20 cm in diameter, 20 cm height) taken from the subsoil (30-50 cm depth). X-ray computed tomography (CT) imaging was used to visualise and quantify soil pore structures in the soil columns. The degree of preferential water flow (5% arrival time, $t_{0.05}$) was calculated from non-reactive tracer breakthrough curves. Saturated hydraulic conductivity ($K_s$) and air permeability ($K_a$) at field moisture content were also measured. The soil macroporosity values derived from CT images were then related to air permeability, 5% arrival time and saturated hydraulic conductivity, to get a better understanding of pore system functioning. The hypothesis tested in Paper I was that soil compaction increases the presence of preferential flow.

## 2.2 Paper II: Compaction effects on flow patterns

In Paper II, the aim was to quantify the effects of compaction on water flow patterns at the soil profile scale. Because of the interaction between the natural recovery processes and induced compaction, quantifying soil compaction effects on water flow patterns is challenging, This complexity means that the impacts

of compaction on water flow patterns in agricultural soils are still poorly understood. One year after establishing the compaction treatment, dye tracing experiments were performed and a range of soil mechanical and hydraulic properties (*i.e.* penetration resistance, bulk density, macroporosity and mesoporosity) were measured, to help explain the dye patterns.

# 3 Materials and Methods

The same field experiments were used in Paper I and Paper II, and therefore the site description and experimental design are identical for both papers.

## 3.1 Site description and experimental design

The compaction experiments were carried out at two field sites (Upper and Lower, approximately 300 m apart) on a well-structured clay soil (45-54% clay) close to Uppsala in central Sweden. The groundwater level at the sites is regulated by a nearby stream and is approximately 50 cm higher at the Upper site than at the Lower site. Detailed information about the two sites can be found in Papers I and II. Some basic properties of the soils at the sites are presented in Table 1.

Table 1. *Soil texture and organic matter content of soils from the Upper and Lower experimental sites used in Papers I and II*

| Site | Sampling depth | Particle size distribution (%) | | | Organic matter content (%) |
|------|------|------|------|------|------|
| | | Clay (<0.002 mm) | Silt (0.002-0.06 mm) | Sand (0.06-2 mm) | |
| Upper | 15 cm | 47.3 | 31.5 | 21.2 | 3.5 |
| | 30 cm | 46.5 | 32 | 21.5 | 1.3 |
| | 50 cm | 46.5 | 35.3 | 18.2 | 0.3 |
| Lower | 15 cm | 50 | 30 | 20 | 3 |
| | 30 cm | 50.5 | 32.5 | 17 | 0.3 |
| | 50 cm | 53.8 | 32.5 | 13.7 | 0 |

Two randomised complete block trials were designed, with two treatments (compacted and control), four blocks of two plots at each site and plot size 9 m × 20 m (Figure 1).
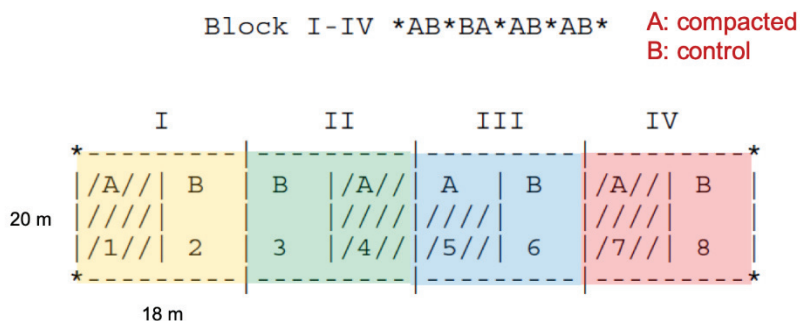


Figure 1. Randomized block design used at both the Upper and Lower sites, with four blocks (1-4) and two treatments (A, B) in eight plots (1-8).

The compaction treatment was performed by four passes with a three-axle dumper truck (Bell B25D 6×6) with 5.8, 5.4 and 4.6 Mg wheel load on the first, second and third axle and 420 kPa tyre inflation pressure (tyre size: 23.5R25) (Figure 2). After compaction, both sites were mouldboard ploughed to a depth of approximately 20 cm. An oat crop was grown at both sites, with seedbed preparation and sowing in spring and harvest at the end of August.



Figure 2. Experimental compaction treatment involving four passes with a 5-ton wheel load dumper truck.

One year after the compaction treatment, soil column/core sampling and field measurements were carried out, at a time when the soil was slightly wetter than field capacity.

## 3.2   Sampling

32 large soil columns (20 cm height, 20 cm diameter), were extracted from the 30-50 cm soil layer in compacted and control plots at the Upper and Lower sites (two per plot). After sampling, the soil columns were tightly closed at both ends to avoid evaporation and were stored at 1 °C to prevent earthworm activity until measurements. Before starting the laboratory measurements, the tops and bottoms of the soil columns were carefully trimmed with the point of knife to reveal undisturbed soil. These soil columns were used for CT imaging, solute breakthrough experiments and hydraulic conductivity measurements in Paper I.

For measurements in Paper II, in September 288 small soil cores (5 cm height, 7.2 cm diameter) were extracted from three depths (10, 30 and 50 cm) in compacted and control plots at the two sites (Figure 3).



*Figure 3.* Sampling of small soil cores (5 cm height, 7.2 cm diameter) in field plots.

On arrival at the laboratory sampling, the soil cores were gradually saturated from the base. Half of the soil cores (n=144) were used for measurements of

saturated hydraulic conductivity and the other half for water retention and bulk density measurements.

## 3.3   Computed tomography (CT) imaging (Paper I)

A medical CT scanner with pore resolution 1.2 mm diameter was used to produce CT images of the soil columns (Figure 4). Detailed information about the method and image analyses can be found in Paper I.
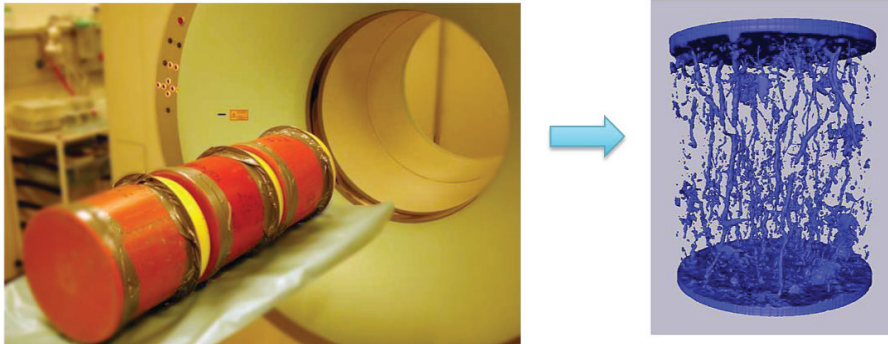


*Figure 4.* (Left) Use of a medical computed tomography (CT) scanner to visualise the pore system in soil columns and (right) example of a CT image. Photo by Mathieu Lamandé.

Macroporosity, connected porosity and total number of individual macropore clusters (no. of pores) were calculated from the CT images.

## 3.4   Solute breakthrough curve (BTC) (Paper I)

Solute breakthrough experiments on large soil columns from the Upper site were carried out in a laboratory irrigation chamber (constant rate, 5 mm h$^{-1}$). Because of very low hydraulic conductivity at the Lower site, the solute breakthrough experiment on those soil columns was carried out under ponding conditions (Figure 5). The electrical conductivity of the effluent was logged at 1-minute intervals using electrical conductivity meters, to provide breakthrough curves (BTCs). From these BTCs, the relative 5%-arrival time $t_{0.05}$ (-), was derived. Detailed information about the method and analyses can be found in Paper I.

*Figure 5.* Equipment used for breakthrough experiments under ponding conditions on soil columns from the Lower site (Paper I).

## 3.5 Saturated hydraulic conductivity ($K_s$) (Paper I)

The saturated hydraulic conductivity, $K_s$, of each column was measured using the falling-head method according to Jury *et al.* (1991), with an initial ponding height at the soil surface of 20 cm (Figure 6). Saturated hydraulic conductivity for the large columns was then calculated as:

$$Ks = \left(\frac{L}{t1}\right) Ln \left(\frac{b0 + L}{b1 + L}\right)$$

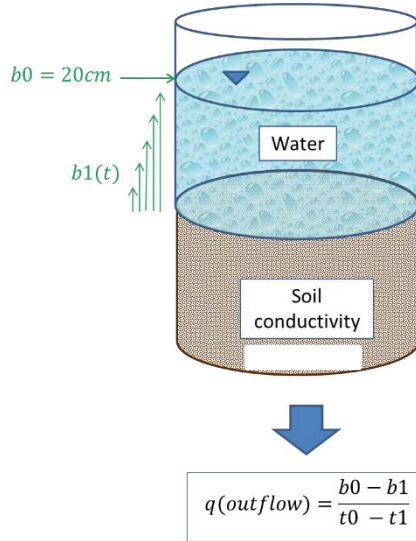where $L$ is cylinder height (20 cm), $b0$ is initial water level (20 cm) and $b1$ is water level at time $t1$.

*Figure 6.* Schematic diagram of the falling head test used for measuring saturated hydraulic conductivity (K$_s$) on soil columns (Paper I).
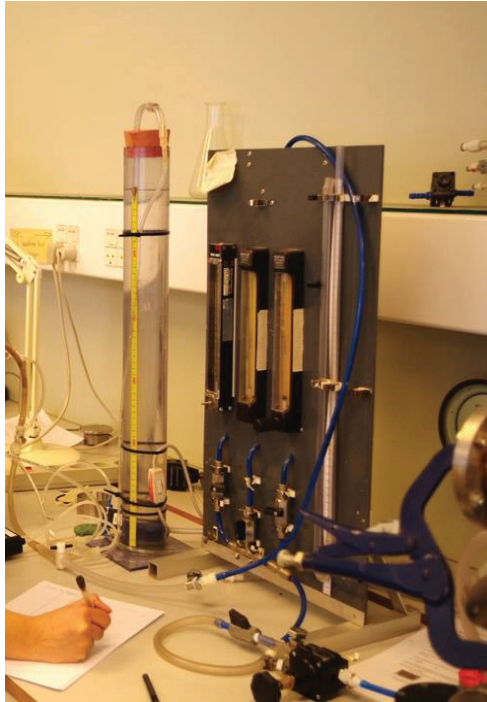
## 3.6  Air permeability (K$_a$) (Paper I)

Air permeability (K$_a$) of the soil columns at field water content was measured using the method developed by Iversen *et al.* (2001). The volumetric air flow rate through the soil columns was recorded and the air permeability was then calculated from Darcy's law (Figure 7).

Air permeability is defined as the rate of airflow passing perpendicularly through a known area under a prescribed air pressure differential between the two surfaces of a material. It is calculated as:

$$K_a = \frac{q_v \times \mu \times L_s}{\rho \times g \times A_s \times h}$$

where $K_a$ is air permeability ($\mu m^2$), $q_v$ is air flow, µ is viscosity of air, g is acceleration due to gravity, ρ is density of water, $L_s$ is sample height (in this case 20 cm), $A_s$ is sample area and h is manometer reading (in this case 5 hPa).

*Figure 7.* Air permeability measurement at the Department of Agroecology, Aarhus University (Paper I).

## 3.7 Bulk density and saturated hydraulic conductivity in small soil cores (Paper II)

Bulk density and saturated hydraulic conductivity ($K_s$) were measured on small soil cores (5 cm height, 7.2 cm diameter) taken from three depths (10, 30 and 50 cm) in all plots (1-8) at both sites (Upper, Lower). More details about the methods can be found in Paper II.

## 3.8 Water retention (Paper II)

Water retention was measured on small soil cores (5 cm height, 7.2 cm diameter) using the sand-box method (Eijkelkamp, model 102 08.01). From the water contents measured at saturation and at tensions of 10, 50 and 100 hPa, the volume of macropores (equivalent pore diameter >0.3 mm), large mesopores (0.3-0.06 mm) and small mesopores (0.06-0.03 mm) was obtained. Finally, the samples were oven-dried, and bulk density and volumetric water content at each tension step were calculated. More details about the methods can be found in Paper II.

## 3.9   Penetration resistance in the field (Paper II)

Soil penetration resistance was measured in the field using a hand-held Eijkelkamp penetrologger with a cone with 1 cm$^2$ base area and 60° apex angle. Measurements were made to 50 cm depth at 15 randomly selected locations per plot. A soil penetrometer measures the soil resistance to penetration, expressed as the force per unit cross-sectional area of the cone base (Bengough *et al.*, 2001). The penetrometer is a useful tool for quickly evaluating the presence of compacted layers in the field (Minasny, 2012).

## 3.10  Dye tracing test in the field (Paper II)

For the dye tracing test, a 1 m$^2$ area in each plot was first irrigated with 20 L of water using a watering can. After 24 hours, 30 L of Brilliant Blue solution (4 g L-1) were applied. Three vertical soil profiles in each plot were then excavated to a depth of 150 cm, and the profile walls were carefully prepared with knives (see Figure 8 and Figure 9).



*Figure 8.* Excavation of dye tracing profiles during the dye tracing tests at the field sites.

*Figure 9.* Preparing profile walls for photographing dye pathways during the dye tracing test.

The plots were then photographed under both sunny and cloudy conditions, to provide different dye tracing images (see Figure 10 and Figure 11). At the Upper site, photographs taken from the soil surface down to 100 cm were analysed, whereas at the Lower site photographs taken from the soil surface down to only 70 cm depth were analysed, because of differences in groundwater levels at the two sites.

*Figure 10.* Example of dye tracing images taken under (left) sunny and (right) cloudy conditions.
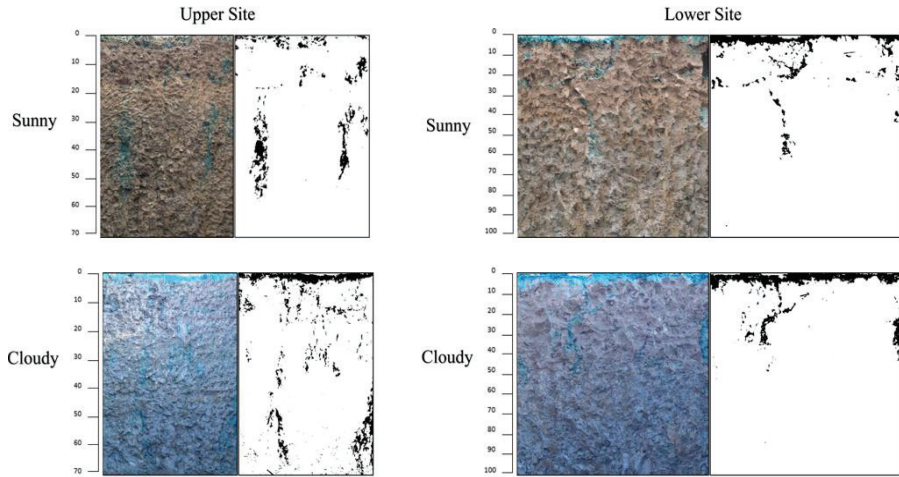


*Figure 11.* Examples of dye tracing images used for analysis of flow patterns at (left) the Upper site and (right) the Lower site under (top row) sunny and (bottom row) cloudy conditions.

Fraction of profile area dyed and number of stained flow paths were derived after image processing and calculation in Matlab. Full details of image processing and calculations can be found in Paper II.

## 3.11 Statistical analysis

All statistical analyses were performed using the JMP-10/JMP pro-11 software. Significant differences between means were determined by Student's t-test, with p-values less than 0.05 considered statistically significant. Log-transformed of $K_s$ and $K_a$ values were used in all statistical analyses, since the measured data covered more than two orders of magnitude and were not normally distributed. More details about the statistical analyses can be found in Papers I and II.

# 4 Results and Discussion

This chapter presents selected results and discusses the main findings from Papers I and II. For a complete description of the results, see the relevant sections in Papers I and II.

## 4.1 Compaction effects on soil pore structure and transport properties

A summary of pore structure characteristics and transport properties ($K_a$, $K_s$ and $t_{0.05}$) at the two sites is presented in Table 2. The table shows only data for 30 cm depth, because the compaction effects were most pronounced at this depth. Results from other depths studied and comparisons between these can be found in Paper II.

As can be seen in Table 2, macroporosity at the Lower site was in general smaller than at the Upper site. The compaction treatment caused a significant decrease (from 4.0% to 1%; p=0.03) in large mesopores (0.3-0.06 mm) at the Upper site. There was also a tendency for smaller percentages of pores ≥0.03 mm, large macropores ≥1.2 mm, small macropores ≥0.3 mm and number of pores (No.) in the compacted treatment compared with the control at the Upper site, although these differences were not significant. In contrast, only the number of pores decreased significantly at the Lower site (from 448.6 to 302.8; p=0.04) after compaction.

Compaction was found to significantly decrease both $K_s$ and $K_a$ at the Lower site, which is consistent with the decrease in the number of larger pores (Table 2). The 5% arrival time ($t_{0.05}$) was significantly higher in compacted plots than in control plots at the Lower site, suggesting less preferential flow transport after compaction at that site. At the Upper site, there was a tendency for lower $K_s$ and $K_a$ and higher $t_{0.05}$ in compacted plots, although these effects were not statistically significant. Higher values for $t_{0.05}$ after compaction were also

observed at the Upper site, suggesting that compaction decreased preferential flow/transport at both sites, but with much a stronger impact at the Lower site.

The differences between the two sites in their response to the applied compaction may be related to different pore volumes, as original macroporosity/mesoporosity was smaller at the Lower site than at the Upper site. Considering also the fact that the groundwater level was about 50 cm deeper at the Upper site than the Lower site, this suggests that the soil at the Upper site under grass ley (compared with cereal stubble at the Lower site) was drier at the time of compaction and probably more resistant to compaction.

Table 2. *Summary of pore size distribution, air permeability ($K_a$), saturated hydraulic conductivity ($K_s$), bulk density (Bd) and 5% arrival time ($t_{0.05}$) for soil at 30 cm depth at the Upper and Lower site. *p<0.05 (p-values calculated using log-transformed values for Ka and Ks)*

| Site | Parameters | Sample size[†] | Control | Compacted | p-value |
|------|-----------|------------|---------|-----------|---------|
| Upper | Porosity ≥0.03 mm | S | 8.0% | 4.0% | 0.07 |
| | Large macropores ≥1.2 mm | L | 0.46% | 0.35% | 0.28 |
| | Small macropores ≥0.3 mm | S | 4.0% | 2.0% | 0.3 |
| | Large mesopores (0.3-0.06 mm) | S | 4.0% | 1.0% | 0.003* |
| | Small mesopores (0.06-0.03 mm) | S | 1.0% | 0.9% | 0.1 |
| | No. of pores ≥1.2 mm | L | 642.3 | 518.7 | 0.37 |
| | Bd (g cm$^{-3}$) | S | 1.31 | 1.38 | 0.09 |
| | Ka (µm$^2$) | L | 33.5 | 21.0 | 0.14+ |
| | Ks (cm h$^{-1}$) | L | 37.7 | 32.0 | 0.28+ |
| | $t_{0.05}$ (-) | L | 0.14 | 0.16 | 0.66 |
| | Porosity ≥0.03 mm | S | 1.0% | 1.0% | 0.82 |
| Lower | Large macroporosity ≥1.2 mm | L | 0.16% | 0.09% | 0.10 |
| | Small macroporosity ≥0.3 mm | S | 0.1% | 0% | 0.52 |
| | Large mesopores (0.3-0.06 mm) | S | 1.0% | 1.0% | 0.84 |
| | Small mesopores (0.06-0.03 mm) | S | 0.3% | 0.8% | 0.04* |
| | No. of pores ≥1.2 mm | L | 448.6 | 302.8 | 0.004* |
| | Bd (g cm$^{-3}$) | S | 1.37 | 1.46 | 0.08 |
| | Ka (µm$^2$) | L | 12.1 | 4.0 | 0.02* |
| | Ks (cm h$^{-1}$) | L | 10.9 | 0.09 | 0.05* |
| | $t_{0.05}$ (-) | L | 0.13 | 0.25 | 0.02* |

[†]*L: Measurements on soil columns (20 cm height and 20 cm diameter) taken at 30-50 cm depth.*

*S: Measurements on small cores (5 cm height, 7.2 cm diameter) at 30 cm depth.*

## 4.2 Relationship between soil pore structure and transport properties

Saturated hydraulic conductivity and air permeability were significantly correlated at both sites (Figure 12), as could be expected from a theoretical perspective (Ghanbarian *et al.*, 2014).
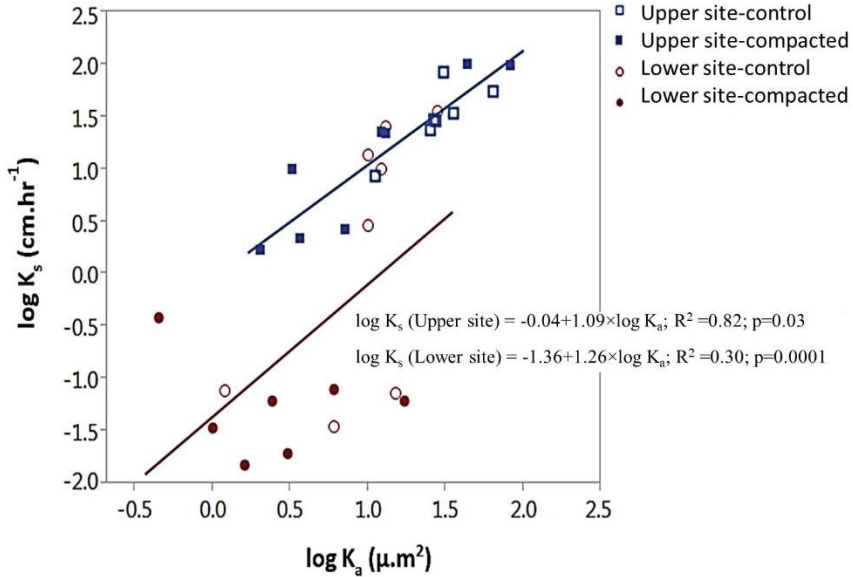


*Figure 12.* Relationship between air permeability ($K_a$) and saturated hydraulic conductivity ($K_s$) in soil from control and compacted plots at the Upper and Lower sites.

Saturated hydraulic conductivity was significantly correlated with large macropores $\geq 1.2$ mm and decreased rapidly as the imaged macroporosity decreased from 0.3% towards zero, especially at Lower site (Figure 13). This means that water flow was strongly limited when the porosity was less than 0.3%. The correlation between $K_s$ and connected porosity $\geq 1.2$ mm is shown in Figure 14.

*Figure 13.* Relationship between saturated hydraulic conductivity (Kₛ) and percentage of macropores ≥1.2 mm determined from computed tomography (CT) images of large soil columns taken from control and compacted plots at the Upper and Lower sites..



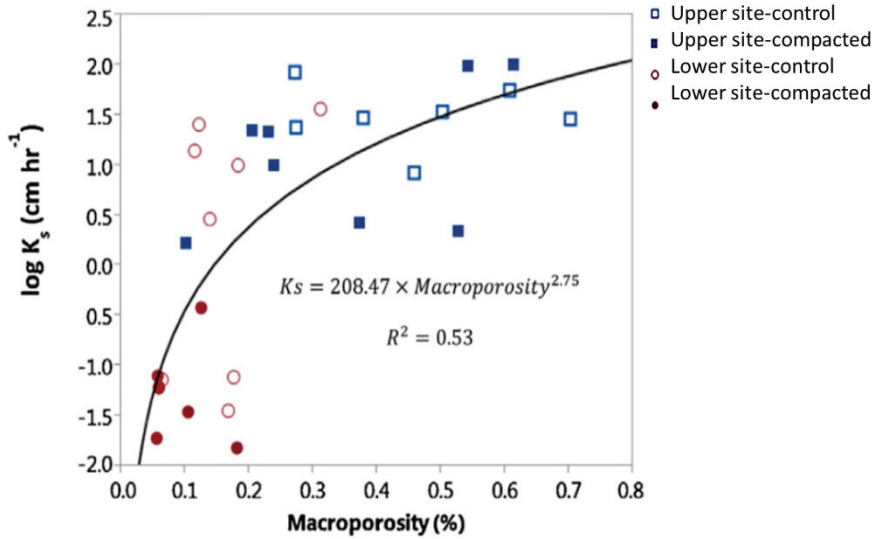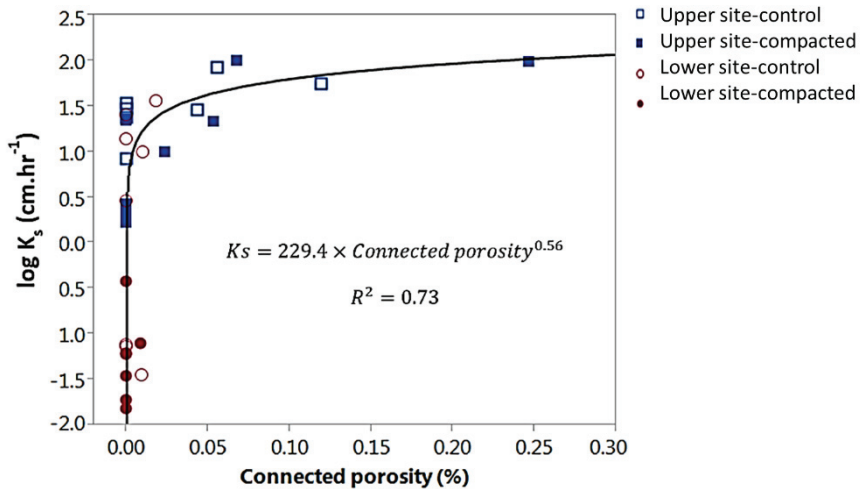*Figure 14.* Relationship between saturated hydraulic conductivity (Kₛ) and percentage of connected pores determined from computed tomography (CT) images of large soil columns taken from control and compacted plots at the Upper and Lower sites.

The wide variation in $K_s$ (from 0.06 to 34 cm hr$^{-1}$) observed in the large soil columns showed no association with connected porosity determined from CT images (Figure 14). Macroporosity in these columns varied from 0.18% to 0.5% (see Tables 2 and 3 in Paper I). It can be suggested that variation in $K_s$ in these columns depended on connected porosity below the image resolution of X-ray CT (1.2 mm).

Data on $K_s$ and porosity larger >0.03 mm measured on small soil cores (see Paper II for details) at both sites and all depths were used to check this suggestion. As shown in Figure 15, there was a linear relationship between $\log K_s$ and the volume of pores >0.03 mm in diameter. Comparing Figure 14 and Figure 15 suggests that transport functions were mostly governed by pores between 0.03-1.2 mm in diameter at both sites. This is an interesting finding, which may suggest that these pores (0.03-1.2 mm) are those most active in preferential flow/transport in this structured clay soil.
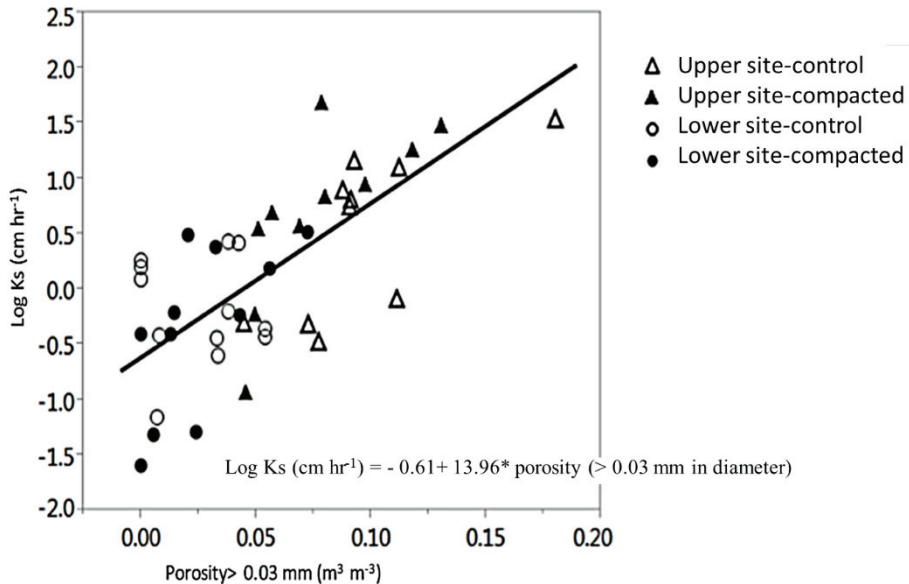


*Figure 15.* Saturated hydraulic conductivity ($K_s$) as a function of fraction of pores larger than 0.03 mm (corresponding to macropores, large mesopores and small mesopores) in soil from control and compacted plots at the Upper and Lower sites.

## 4.3   Compaction effects on preferential flow

The 5% arrival times for control plots at both sites were relatively small (0.14 at Upper site and 0.13 at Lower site), which according to Koestel *et al.* (2012)

indicates strong preferential flow. At the Lower site, compaction caused significant increases in $t_{0.05}$ (to 0.25), which means that compaction limited the strength of preferential flow at that site (Table 2). At the Upper site, no significant effect of compaction on preferential flow was found, although $t_{0.05}$ values were generally larger in the compacted treatment than control (mean 0.16 vs 0.14) (Table 2).

An inverse relationship between $t_{0.05}$ and macroporosity was found at the Lower site, whereas no trend was obvious at the Upper site (Figure 16). Loss of macroporosity due to compaction at the Lower site may have decreased preferential flow by reducing macropore continuity (Jarvis, 2007). This effect was apparent as the connected porosity was greater in control plots than in compacted plots at the Lower site (see Table 2 in Paper I). It can be therefore concluded that the effect of compaction on preferential flow may be attributed partly to a reduction in the volume and continuity of macropores smaller than 1.2 mm in diameter, which was the resolution of the CT scanner used in the present work.
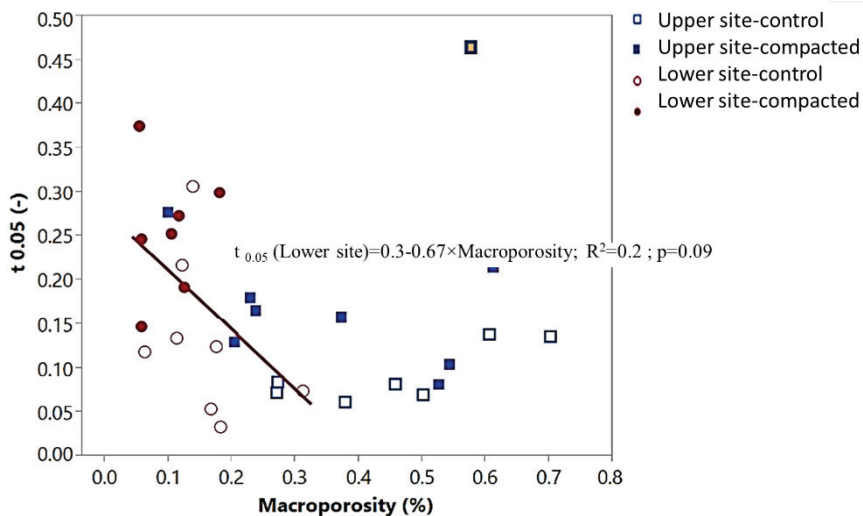


*Figure 16.* Relationship between 5% arrival time ($t_{0.05}$) and macroporosity in soil from control and compacted plots at the Upper and Lower sites. The high $t_{0.05}$ value for a control plot at the Upper site (square orange icon) was considered an outlier caused by an earthworm channel passing through the entire column, which resulted in rapid throughflow.

These results contradict those reported by Katuwal *et al.* (2015), who found a significant positive correlation between $t_{0.05}$ and macroporosity derived from CT images with similar image resolution as in this thesis. The samples analysed

in that study were taken from an agricultural field in Denmark with low (14.7-18.2%) clay content, whereas the samples analysed in this thesis had a much higher (45-54%) clay content. All samples analysed by Katuwal *et al.* (2015) had macroporosity greater than ~0.4%, while the columns studied in this thesis had much smaller values (see Tables 2 and 3 in Paper I). Larsbo *et al.* (2014) also found a higher degree of preferential flow (*i.e.* smaller $t_{0.05}$ values) in topsoil samples with lower CT image macroporosity and saturated hydraulic conductivity. In marked contrast to the narrow range of macroporosity (~0.1-0.5%) observed for soil columns in this thesis, macroporosity values in the soils studied by Larsbo *et al.* (2014) were higher and showed greater variation (range ~3 to 10%). Taken together, these findings suggest that, as hypothesised by Jarvis (2007), moderate compaction should increase the strength of preferential flow as macroporosity decreases but a few continuous macropores remain. As compaction becomes more severe, a critical point is reached at which pore continuity limits preferential flow. At this point, the saturated hydraulic conductivity of the soil may become so small that surface runoff may occur, depending on the surface boundary conditions in the field.

## 4.4 Dye patterns and penetration resistance one year after compaction

At both sites, penetration resistance increased markedly below 25 cm depth, indicating the presence of a compacted layer at this depth, even in the control treatment (Figure 17). The compaction treatment applied resulted in significantly higher penetration resistance (compared with the control) at 5-10 cm depth (p=0.04), 10-15 cm depth (p=0.052) and 15-20 cm depth (p=0.05) at the Lower site (Figure 17, right). In contrast, at the Upper site, penetration resistance was not significantly affected by compaction of the topsoil. The compacted plots at the Upper site tended to have higher penetrometer resistance in the subsoil (40-50 cm depth) (Figure 17, left), but these differences were not statistically significant (p=0.09 at 40-45 cm; p=0.08 at 45-50 cm).
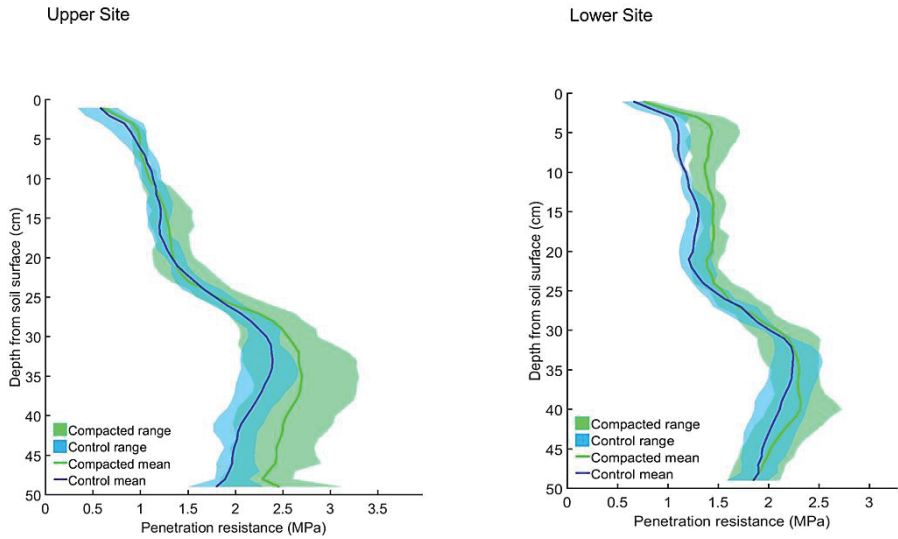
*Figure 17.* Penetration resistance patterns in soil at (left) the Upper site and (right) the Lower site before compaction (blue) and after compaction (green).

The results from the penetration resistance and dye tracing tests in the field suggest the presence of a compacted layer at about 20-30 cm depth at both sites (compare Figure 18 and Figure 17). The presence of this compacted layer was obvious at the Lower site from dye tracing, where the dyed area was mostly concentrated above 30 cm depth.
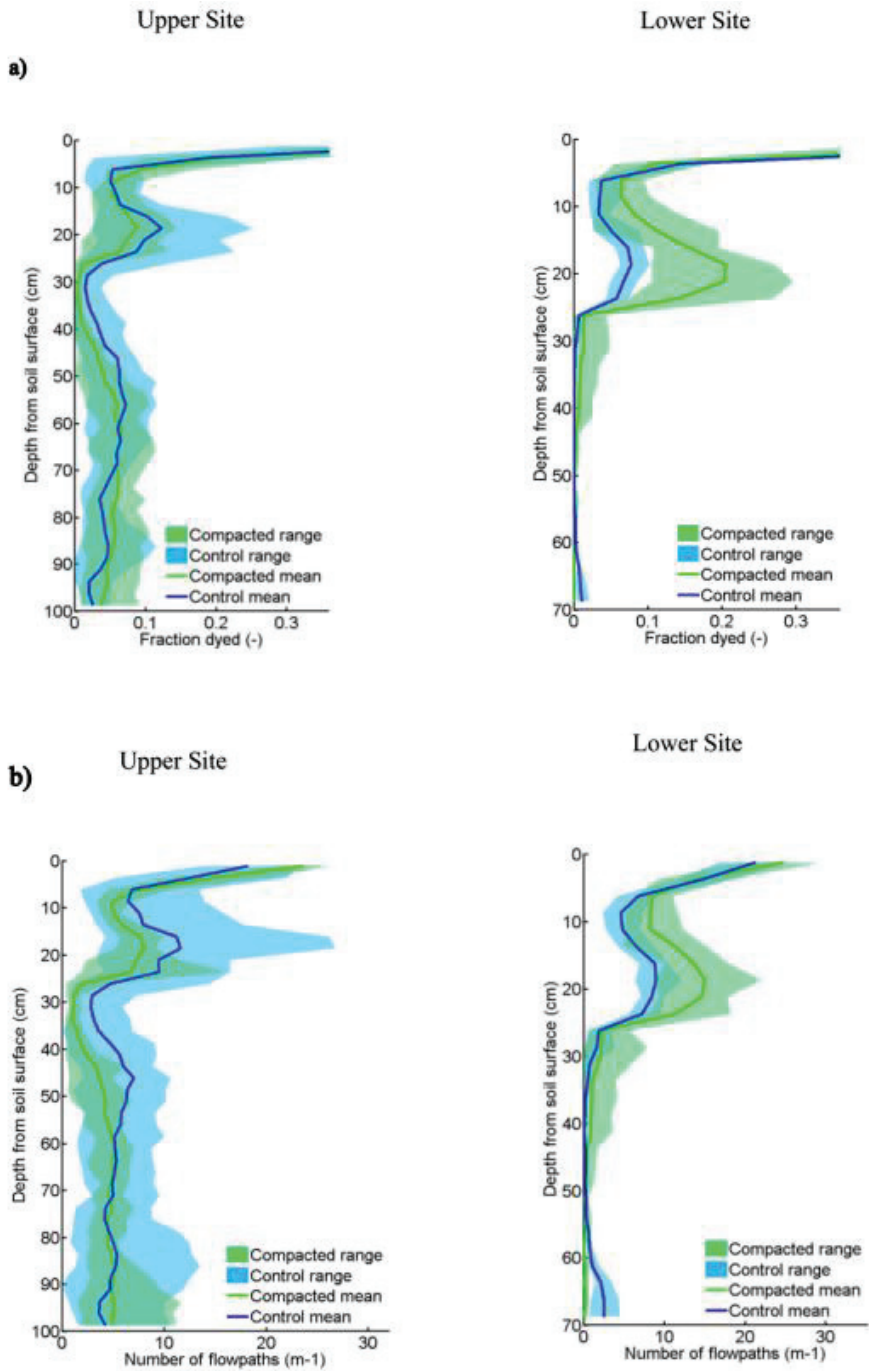
*Figure 18.* (a) Fraction of the soil profile dyed and (b) number of stained flow paths in control and compacted field soil at (left) the Upper site and (right) the Lower site.

Compaction led to a smaller dyed area (Figure 18a, left) and a smaller number of flow paths (Figure 18b, left) in the whole soil profile at the Upper site. At the Lower site, compaction resulted in a clear increase in the dyed area at 5-25 cm depth, with very little dyed area observed below 25 cm depth in both compacted and control plots at that site (Figure 18a, right). At the Lower site, ponding at the soil surface was observed during the dye tracing experiments, especially in the compacted plots, which supports the conclusion that water transport was limited due to the presence of a compacted layer (25 cm depth) characterised by greater penetration resistance. However, the ponding conditions at the Lower site did not induce any noticeable preferential transport of the dye solution deep into the subsoil (*Figure 19)*. This observation is consistent with our earlier findings for large columns (30-50 cm depth) taken at the Lower site, where almost no continuous macroporosity was found based on CT images (Mossadeghi-Björklund *et al*., 2016). However, the findings for the Lower site partly contradict those of Kulli *et al*. (2003), who reported larger dyed area in the subsoil because of compaction. They suggested that a decrease in permeability of the topsoil, caused by compaction, led to local ponding and enhanced preferential flow through remaining continuous macropores into the subsoil. Bogner *et al.* (2013) also found larger dyed area in the plough layer (25-30 cm depth) and concluded that flow transport above the plough layer was partly disconnected from the subsoil because of macropore disruption by tillage. However, in their study, preferential flow along cracks occurred in both compacted and control plots and the disconnected macropores below the plough layer still functioned as preferential flow paths (Bogner *et al*., 2013). This was not observed at the Lower site in this thesis, probably because there were not enough continuous macropores that could support preferential flow in the subsoil (Jarvis *et al*., 2016, 2017).
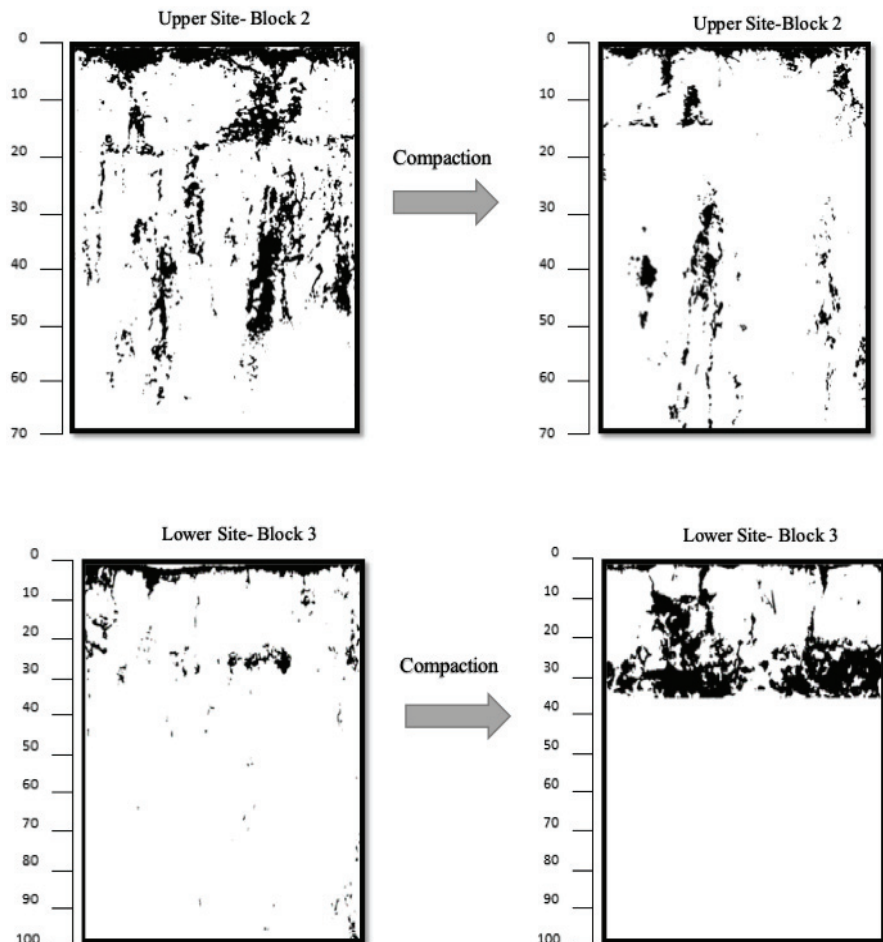
*Figure 19.* Examples of the effect of compaction on tracer dye flow pattern in soil in two treatment blocks at (top row) the Upper site and (bottom row) the Lower site.

An illustrative explanation of how compaction influenced flow transport at Upper site and Lower site is presented in Figure 20. As can be seen from the diagram, there was a clear decrease in preferential flow below the compacted layer (plough pan) in compacted plots, especially at the Lower site. This observation is consistent with our previous results for large soil columns (Mossadeghi-Björklund *et al.*, 2016), where compaction resulted in significantly higher $t_{0.05}$ (less preferential flow).
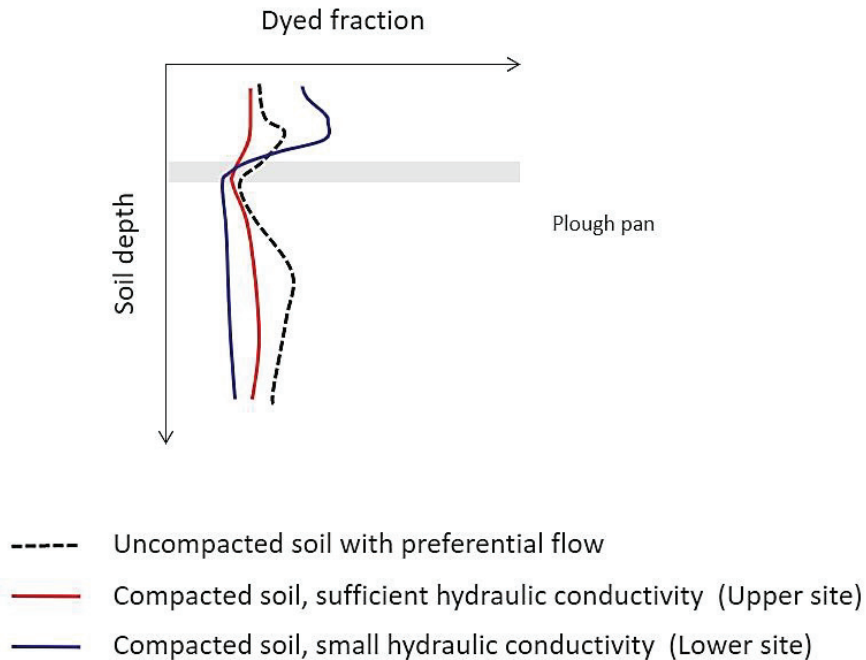
*Figure 20.* Illustration based on dye tracing images (*Figure 18*) of how compaction influenced flow paths in uncompacted and compacted soil at the Upper and Lower sites.

This reasoning is summarised in the conceptual model presented in Figure 21, which illustrates how preferential flow and surface runoff may be affected by compaction and natural regeneration of soil structural macropores (*e.g.* due to cracking or earthworm activity) following compaction. According to the model, moderate compaction may induce stronger preferential flow due to a decrease in near-saturated hydraulic conductivity and an increase in the size of the largest conducting pores (compared curve B with curve A in Figure 21). More severe compaction may result in an increased risk of surface runoff and weaker preferential flow, since the size of the largest pores in the soil is dramatically decreased (curve C in Figure 21). Larger soil macropores such as cracks and earthworm channels may subsequently regenerate, while the recovery of smaller pores affected by compaction is a slower process. This may lead to very strong preferential flow (curve D in Figure 21).

*Figure 21.* Conceptual model of preferential flow as influenced by soil compaction and subsequent recovery from compaction. A: no compaction, B: intermediate compaction, C: strong compaction, D: regeneration of macropores after compaction.

# 5 Conclusions

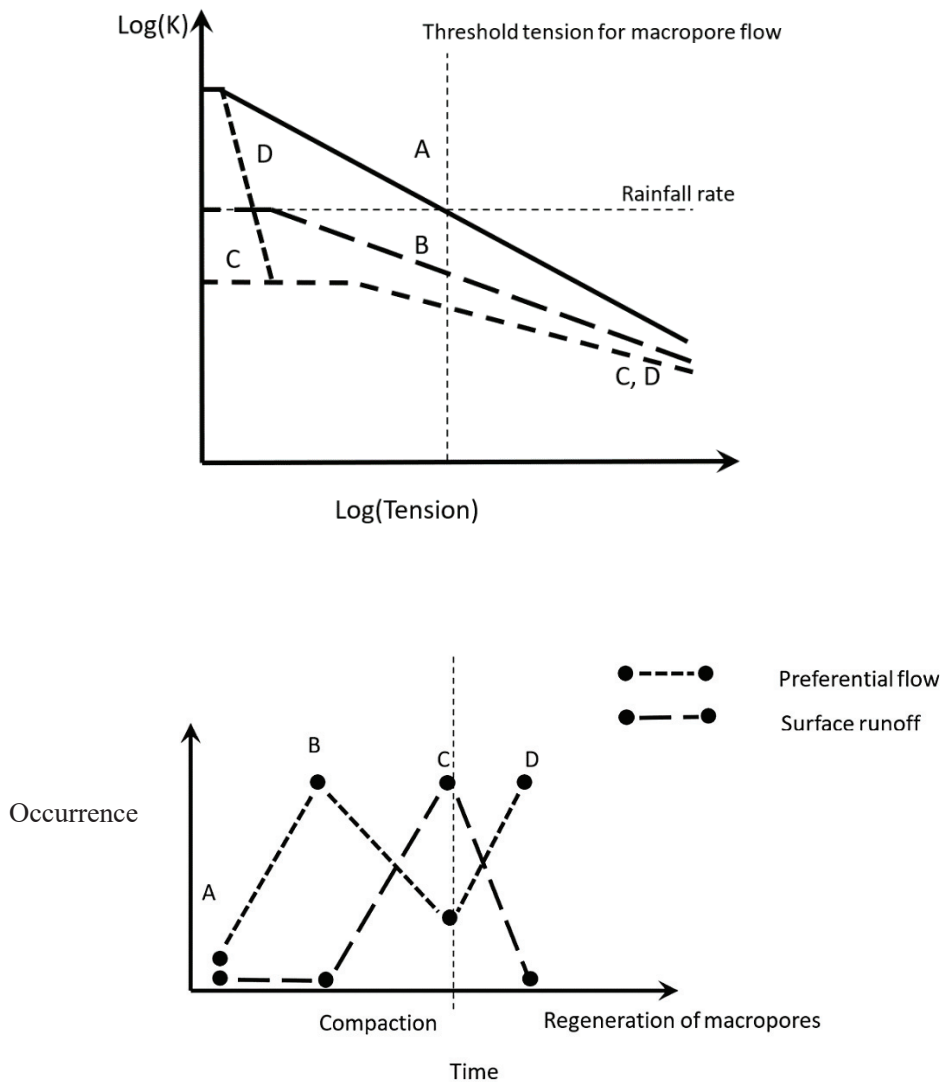Significant effects of compaction on structural pore space (macroporosity) were found at 25-30 cm depth (compacted layer), with pronounced limitation of flow and transport below this depth. Both soils were ploughed after the compaction treatment, so the presence of a compacted layer indicates that ploughing did not remove the negative effects of compaction at 25-30 cm depth. Such subsoil compaction is an issue in many agricultural soils with a high clay content as it can lead to flood generation and runoff, a serious problem for farmers. This thesis showed that even quite small differences in initial soil and site conditions may significantly influence the extent to which applied compaction stresses affect the connectivity of structural pore space in soil and, consequently, water flow. To prevent subsoil compaction, it is important to consider soil conditions at the time of trafficking.

The neighbouring sites studied in this thesis had strong preferential flow in control plots. Water flow through preferential flow pathways can facilitate transport of fertilisers, pesticides, and contaminants to groundwater, causing harmful environmental problems. Since groundwater is used as drinking water, leaching of contaminants to groundwater may also affect human health.

Based on the results, a conceptual model was developed. It suggests that preferential flow is strongest at some intermediate level of compaction, at which macropore continuity is still maintained despite reductions in macroporosity. It also illustrates how compaction and subsequent recovery from compaction may affect soil susceptibility to preferential flow and surface runoff.

# References

Alaoui, A., Goetz, B. (2008). Dye tracer and infiltration experiments to investigate macropore flow. *Geoderma* 144: 279-286.

Alaoui, A., Lipiec, J., Gerke, H.H. (2011). A review of the changes in the soil pore system due to deformation: A hydrodynamic perspective. *Soil Tillage Res*, 115-116: 1-15.

Allaire, S.E., Roulier, S., and Cessna, A.J. (2009). Quantifying preferential flow in soils: A review of different techniques. *J. Hydrol,* 378: 179– 204.

Arvidsson, J., Håkansson, I. (1996). Do effects of soil compaction persist after ploughing, Results from 21 long-term field experiments in Sweden. *Soil Tillage Res*, 39: 175-198.

Arvidsson, J. (1997). Soil compaction in agriculture- from soil stress to plant stress. Doctoral thesis. Department of soil and Environment, SLU. *Agraria* 41.

Bengough, A.G., Campbell, D.J., and O'Sullivan, M.F. (2001). Penetrometer techniques in relation to soil compaction and root growth. In Smith, K.A. and Mullins, C.E., Eds. *Soil and Environmental Analysis: Physical Methods*, 2nd ed., Marcel Dekker, New York, NY. pp. 377-403.

Bogner, C., Mirzaei. M., Ruy, S., Huwe, B. (2013). Microtopography, water storage and flow patterns in a fine-textured soil under agricultural use. *Hydrol. Process,* 27: 1797–1806.

Cassaro, F.A.M., Borkowski, A., Pires, L., Rosa, J., Saab, S. (2011). Characterization of a Brazilian clayey soil submitted to conventional and no-tillage management practices using pore size distribution analysis. *Soil Tillage Res,* 111: 175-179.

Chamen, W.C.T., Moxey, A.P., Towers, W., Balana, B., Hallet, P.D. t. (2015). Mitigating arable soil compaction: a review and analysis of available cost and benefit data. *Soil Tillage Res*, 146: 10-25.

Etana, A., Håkansson, I. (1994). Swedish experiments on the persistence of subsoil compaction caused by vehicles with high axle load. *Soil Tillage Res*, 29: 167-172.

Ghafoor, A., Jarvis, N.J., Stenström, J. (2013). Modelling pesticide sorption in the surface and subsurface soils of an agricultural catchment. *Pest Management Science*, 69: 919-929.

Ghanbarian, B., Hunt, A.G., Ewing, R.P., Skinner, T.E. (2014). Theoretical relationship between saturated hydraulic conductivity and air permeability under dry conditions: Continuum percolation theory. *Vadose Zone Journal*, 13: 1-6.

Goulding, K.W.T., Poulton, P.R., Webster, E.P., Howe, M.T. (2000). Nitrate leaching from the Broadbalk Wheat Experiment, Rothamsted, UK, as influenced by fertilizer and manure inputs and the weather. *Soil Use Manage*, 16: 244– 250.

Hendrickx, J.M.H., Flury, M. (2001). Uniform and preferential flow mechanisms in the vadose zone. In: *Conceptual models of flow and transport in the fractured vadose zone*. National academy press., Washington, D.C. pp.149-187.

Iversen, B.V., Moldrup, P., Schjonning, P., Loll, P. (2001). Air and water permeability in differently textured soils at two measurement scales. *Soil Science*, 166: 643-659.

Janssen, M., Lennartz, B. (2008). Characterization of preferential flow pathways through paddy bunds with dye tracer tests. *Soil Science Society of America Journal*, 72: 1756-1766.

Jarvis, N.J. (2007). A review of non-equilibrium water flow and solute transport in soil macropores: Principles, controlling factors and consequences for water quality. *European Journal of Soil Sciences*, 58: 523-546.

Jarvis, N., Koestel, J., Larsbo, M. (2016). Understanding preferential flow in the vadose zone: recent advances and future prospects. *Vadose Zone Journal*, 15 (12): 1-11.

Jury, W. A., Gardner, W. R., Gardner, W. H. (1991). *Soil physics: Water movement in soil*. fifth ed. John Willey & Sons, NY. pp.73-121.

Katuwal, S., Norgaard, T., Moldrup, P., Lamande, M., Wildenschild, D., de Jonge, L.W. (2015). Linking air and water transport in intact soils to macropore characteristics inferred from X-ray computed tomography. *Geoderma*, 237: 9-20.

Kim, H., Anderson, S.H., Motavalli, P.P., Gantzer, C.J. (2010). Compaction effects on soil macropore geometry and related parameters for an arable field. *Geoderma*, 160: 244-251.

Knudby, C., Carrera, J. (2005). On the relationship between indicators of geostatistical, flow and transport connectivity. *Advances in Water Resources,* 28: 405-421.

Koestel, J.K., Moeys, J., Jarvis, N.J. (2011). Evaluation of nonparametric shape measures for solute breakthrough curves. *Vadose Zone Journal*, 10: 1261-1275.

Koestel, J.K., Moeys, J., Jarvis, N.J. (2012). Meta-analysis of the effects of soil properties, site factors and experimental conditions on solute transport. *Hydrology and Earth System Sciences*, 16: 1647-1665.

Kulli, B., Gysi, M., Flühler, H. (2003). Visualizing soil compaction based on flow pattern analysis. *Soil and Tillage Research*, 70: 29-40.

Lamandé, M., Wildenschild, D., Berisso, F.E., Garbout, A., Marsh, M., Moldrup, P., Keller, T., Hansen, S.B., de Jonge, L.W., Schjonning, P. (2013). X-ray CT and Laboratory Measurements on Glacial Till Subsoil Cores: Assessment of Inherent and Compaction-Affected Soil Structure Characteristics. *Soil Sci*, 178: 359-368.

Larsbo, M., Koestel, J., Jarvis, N. (2014). Relations between macropore network characteristics and the degree of preferential solute transport. *Hydrology and Earth System Sciences*, 18: 5255-5269.

Lipiec, J., Håkansson, I. (2000). Influences of degree of compactness and matric water tension on some important plant growth factors. *Soil Tillage Res,* 53: 87-94.

Lipiec, J., Hatano, R. (2003). Quantification of compaction effects on soil physical properties and crop growth. *Geoderma*, 116: 107-136.

Minasny, B. (2012). Contrasting soil penetration resistance values acquired from dynamic and motor-operated penetrometers. *Geoderma*, 177: 57-62.

Mossadeghi-Björklund, M., Arvidsson, J., Keller, T., Koestel, J., Lamandé, M., Larsbo, M., Jarvis, N. (2016). Effects of subsoil compaction on hydraulic properties and preferential flow in a Swedish clay soil. *Soil Tillage Research*, 156: 91–98.

Mooney, SJ. (2002). Three-dimensional visualization and quantification of soil macroporosity and water flow patterns using computed tomography. *Soil Use & Manage*, 18: 142–151.

Petrovic, A.M., J.E. Siebert, and P.E. Rieke. (1982). Soil bulk density analysis in three dimensions by computed tomographic scanning. *Soil Sci. Soc. Am. J*, 46: 445–450.

Pires, L.F. (2011). Gamma-ray computed tomography to evaluate changes in the structure of a clayey soil due to agricultural traffic. Acta Scientiarum. *Agronomy*, 33: 411-416.

Schwen, A., Lawrence-Smith, G.H.-R.-E.J., Sinton, S.M., Carrick, S., Clothier, B.E., Buchan, G.D., Loiskandl, W. (2011). Hydraulic Properties and the Water-Conducting Porosity as Affected by Subsurface Compaction using Tension Infiltrometers. *Soil Sci. Soc. Am. J*, 75: 822-831.

Servadio, P., Marsili, A., Pagliai, M., Pellegrini, S., Vignozzi, N. (2001). Effects on some clay soil qualities following the passage of rubber-tracked and wheeled tractors in central Italy. *Soil and Tillage Research*, 61: 143-155.

Vanclooster, M., Mallants, D., Vanderborght, J., Diels, J., Van Orshoven, J., Feyen, J. (1995). Monitoring solute transport in a multi-layered sandy lysimeter using time domain reflectometry. *Soil Sci. Soc. Am. J*, 59: 337– 344

Wildenschild, D., Sheppard, A. P. (2013). X-ray imaging and analysis techniques for quantifying pore-scale structure and processes in subsurface porous medium systems. *Advances in Water Resources*. 51: 217-246.

# Acknowledgements

I would like to thank my past main supervisor, the late Johan Arvidsson, who gave me the opportunity to start my research project and carry out my studies at SLU. I wish Johan were here today, he is greatly missed. My deepest thanks to my supervisor, Nick Jarvis, for all his valuable and scientific guidance, revisions and suggestions for improvements throughout my studies, especially during the publication of papers. I have learnt a lot from you, Nick, it was an honour to be your student. Special thanks to my present main supervisor, Thomas Keller, for all his guidance and useful discussions that helped me find my way, and also for his hospitality and our friendship. I would like to thank my co-supervisor Mats Larsbo for his guidance and tips and kindly providing Figures 17 and 18, and to John Koestel for his improving instructions during the breakthrough measurements. Many thanks to Johannes Forkman for excellent help with the statistics and for patiently listening and teaching me when I was lost handling my data. I thank Tomas Rydberg for his support when I was new at SLU and Ararso Etana for helping me in the field. Thanks to Per Schjønning, Mathieu Lamandé and the other nice people at Aarhus University in Denmark for letting me use their soil physics lab to perform some of my measurements. I am also grateful for the support I have received from my co-workers at the Department of Soil and Environment at SLU.

Last, but not least, I thank my parents, Ahmad-Ali Mossadeghi and Tooran Nazari, for letting their little bird find her own ways in life and for all their love. My sincere thanks go to my husband, Per Mossadeghi Björklund, for love, understanding and encouragement throughout this journey. Without your support I could not have managed it, Per. I am grateful to my lovely parents-in-law, Bertil and Monica Björklund, for their support during my studies. And I am so happy and proud to have two fantastic sons, Yosef and Yones Björklund, who understood when their mom needed to work long hours, thanks for giving me such energy and love, it kept me going.

# Effects of subsoil compaction on hydraulic properties and preferential flow in a Swedish clay soil

M. Mossadeghi-Björklund[a,*], J. Arvidsson[a], T. Keller[a,b], J. Koestel[a], M. Lamandé[c], M. Larsbo[a], N. Jarvis[a]

[a] Swedish University of Agricultural Sciences, Department of Soil and Environment, P.O. Box 7014, SE-750 07 Uppsala, Sweden
[b] Agroscope, Department of Natural Resources and Agriculture, Reckenholzstrasse 191, CH-8046 Zürich, Switzerland
[c] Aarhus University, Department of Agroecology, Research Centre Foulum, Box 50, DK-8830 Tjele, Denmark

ABSTRACT

Soil compaction by vehicular traffic modifies the pore structure and soil hydraulic properties. These changes potentially influence the occurrence of preferential flow, which so far has been little studied. Our aim was to study the effect of compaction on soil hydraulic and transport properties in subsoil. A randomized block design trial at two sites on a well-structured clay soil in central Sweden was established. Plots with two levels of compaction were created at both sites, in the following referred to as trafficked and control. The trafficked treatment was created by 4 passes track-by-track with a three-axle dumper with a maximum wheel load of 5.8 Mg. After one year, undisturbed soil columns (20 cm height × 20 cm diameter) from both trafficked and control plots at a depth of 30–50 cm were sampled. The columns were analyzed using X-ray CT imaging, together with measures of the degree of preferential transport derived from non-reactive tracer breakthrough curves and measurements of saturated hydraulic conductivity ($K_s$) and air permeability at the field moisture content ($K_a$).

Although the traffic treatment did not cause any compaction effects at one of the two sites, it did result in significant reductions in saturated hydraulic conductivity, air permeability and number of macropores at the second site. At this site, the traffic also significantly reduced the strength of preferential flow, presumably due to compaction-induced disruption of macropore continuity. In apparent contrast, some previous studies have shown increases in the strength of preferential flow as a result of compaction. We propose a conceptual model to explain these apparently contradictory results, which suggests that preferential flow should be strongest at some intermediate level of compaction.

© 2015 Published by Elsevier B.V.

## 1. Introduction

Compaction is the process by which soil bulk density increases and porosity decreases, for example due to vehicular traffic. Compaction not only reduces total pore volume but also modifies the pore size distribution, geometry, morphology and connectivity of soil pores (e.g., Servadio et al., 2001). Compaction reduces the saturated and near-saturated hydraulic conductivity of soil (Arvidsson, 1997; Schwen et al., 2011) and also leads to poorer aeration and crop growth and an increased risk of surface runoff (Lipiec and Hatano, 2003). Whereas the effects of topsoil compaction may be partly alleviated when the soil is mouldboard ploughed (Arvidsson and Håkansson, 1996), effects of subsoil compaction persist much longer, and may even be more or less permanent (Etana and Håkansson, 1994). Due to its persistence, subsoil compaction is a major concern in agriculture. Although compaction decreases hydraulic conductivity at and close to saturation, it may cause an increase in conductivity at larger water tensions (i.e., water contents below field capacity), due to an improved connectivity between these smaller pores, which may also increase in volume (Lipiec and Hatano, 2003; Lipiec et al., 2009; Richard et al., 2001).

Changes in the characteristics and geometry of structural pore networks following compaction may also significantly influence solute transport in soil, especially the risk of rapid preferential solute transport under near-saturated and saturated conditions in soil macropores (Hendrickx and Flury, 2001; Jarvis, 2007). However, these effects are still poorly understood and the results of the few studies so far that have investigated this question seem contradictory. As compaction mainly disrupts or destroys macropores in soil, it might be expected to reduce the extent of preferential flow. Heitman et al. (2007) found that trafficked areas

of the field showed a slower breakthrough of non-reactive solute. On the other hand, Koestel et al. (2013), Katuwal et al. (2015a) and Soares et al. (2015) found for breakthrough curve experiments on undisturbed soil columns that the strength of preferential transport was positively correlated with bulk density. However, none of these studies investigated the impact of discrete compaction events. Mooney and Nipattasuk (2003) found for sieved and repacked samples that compaction increased preferential flow in a sandy loam, whereas preferential flow was detected at all compaction levels in a clay loam. Dye tracing studies have demonstrated that strong preferential flow may be induced in any macropores remaining after the compaction event or those that are subsequently re-generated due to physical (i.e., swell/shrink) or biological processes (e.g., root growth, faunal activity) (Alaoui and Goetz, 2008; Etana et al., 2013; Janssen and Lennartz, 2008; Kulli et al., 2003). Annual tillage also creates large voids which allow preferential flow and solute fluxes to by-pass denser traffic-compacted zones or clods in the plow layer (Coquet et al., 2005; Janssen and Lennartz, 2008).

Knowledge of the 3-D macropore network structure is essential for a quantitative understanding of the impact of soil compaction on soil susceptibility to rapid preferential flow. There are many methods available to quantify macropore networks in soil, each with their own advantages and disadvantages (Allaire et al., 2009). In this study, we used X-ray tomography to visualize and quantify soil pore structures (Kim et al., 2010; Lamandé et al., 2013; Pires, 2011; Schjønning et al., 2013; Larsbo et al., 2014) in 20 cm diameter soil columns taken from the upper subsoil (i.e., below the depth of tillage at 30–50 cm) of control and trafficked plots at two nearby field sites on a clay soil in Sweden. The imaged soil macroporosity was related to saturated hydraulic conductivity, air permeability and non-reactive tracer breakthrough measured on the same samples.

## 2. Materials and methods

### 2.1. Site description and sampling

Two wheeling experiments were carried out at two field sites on a well-structured clay soil (hereafter denoted as the Upper site and the Lower site) close to Uppsala (59°48′N, 17°39′E), in central Sweden. The two sites were situated approximately 300 m apart. The climate at the site is cold-temperate and semi-humid with an average annual temperature of 5.5 °C and an average annual precipitation of 527 mm (1961–1990). The coldest month is January (mean −4.9 °C) and the warmest is July (mean +16.4 °C). The soil is classified as a Eutric Cambisol in the WRB system and has a strong prismatic structure in the subsoil. The field is cultivated in a rotation dominated by cereals, with barley (*Hordeum vulgare* L.), winter wheat (*Triticum aestivum* L.), oats (*Avena sativa* L.) and spring oilseed rape (*Brassica napus* L.) as the main crops. Some basic soil properties are presented in Table 1. Soil texture was measured by the pipette method and organic matter content was estimated using the loss on ignition method (Schulte and Hopkins, 1996) for both soils.

The experiment was designed as a randomized block trial with 2 treatments (trafficked and control), with 4 blocks at each site, and a plot size of 9 × 20 m. In November 2010, the trafficked treatment was created by four passes track-by-track with a three-axle dumper truck (Bell B25D 6 × 6) with 5.8, 5.4 and 4.6 Mg wheel load on the first, second and third axle and 420 kPa tyre inflation pressure (tyre size: 23.5R25) when the soil was at field capacity. The Upper site was under grass ley at this time, while the surface of the Lower site was covered with cereal stubble following the harvest of the previous crop. After wheeling, both sites were mouldboard ploughed to a depth of approximately 20 cm. In 2011, spring oats was grown on both sites and harvested at the end of August. On 20 September, 32 undisturbed soil columns, 2 from each plot (20 cm height and 20 cm diameter) were sampled from both trafficked and control plots at a depth of 0.3–0.5 m using a tractor-mounted hydraulic press. After sampling, the soil columns were stored at 1 °C until analysis in order to prevent earthworm activity inside the columns. During storage, the soil columns were tightly closed at both ends to restrict evaporation. Before starting the laboratory measurements, the tops and bottoms of the soil columns were carefully trimmed with the point of a sharp-edged knife to reveal undisturbed soil.

### 2.2. Computer tomography imaging

A medical CT-scanner (SIEMENS Biograph Truepoint 64 combined CT/PET) at the Aarhus Hospital in Denmark was used to visualize the macropore system in the large soil columns. A voltage of 120 kV with a flux of 600 mAs and exposure time of 1 s were used to X-ray scan the soil columns. The soil columns were first prepared by removing loose particles on the surface with a vaccum cleaner. The soil columns were scanned at the field moisture content at the time of sampling which was drier than field capacity. The resolution of each horizontal slice was 512 × 512 pixels and each scan contained 300 slices. The voxel size was $0.43 \times 0.43 \times 0.6$ mm. This means that pores less than 1.2 mm in diameter (2 voxels in width) cannot be reliably detected with this CT-scanner.

Images were then analyzed using the Avizo software® (Visualization Sciences Group, Burlington, MA). The PVC cylinders as well as 1 cm of the soil at both ends were cropped from the images. As a result, the region of interest (ROI) was a cylinder 19 cm in diameter and 18 cm in height (volume of 5103.5 cm³) for each column.

Thresholding based on the intensity histogram of the entire sample (at field water content) was used to segment air-filled pore space: the threshold value between air-filled pore space and water-filled pore space or soil matrix was defined as the minimum value of a parabola fitted to the intensity histogram between the peak for air and the peak for water. More details about the method can be found in Lamandé et al. (2013). All segmented objects less than 2 voxels in diameter might be partial voxels (i.e., noise) and therefore were removed from the analysis. Macroporosity was

**Table 1**
Soil texture and organic matter content of the soils from Upper site and Lower site.

| Soil-texture | Layers | Particle size distribution (%) | | | Organic matter (%) |
|---|---|---|---|---|---|
| | | Clay (<0.002 mm) | Silt (0.002–0.06 mm) | Sand (0.06–2 mm) | |
| Upper site-clay | 15 cm | 47.3 | 31.5 | 21.2 | 3.5 |
| | 30 cm | 46.5 | 32.0 | 21.5 | 1.3 |
| | 50 cm | 46.5 | 35.3 | 18.2 | 0.3 |
| Lower site-clay | 15 cm | 50.0 | 30.0 | 20.0 | 3.0 |
| | 30 cm | 50.5 | 32.5 | 17.0 | 0.3 |
| | 50 cm | 53.8 | 32.5 | 13.7 | 0.0 |

calculated as;

$$\text{Macroporosity (\%)} = \frac{\text{Number of voxels categorized as air}}{\text{Total number of voxels in the ROI}} \times 100 \tag{1}$$

The segmented objects (i.e., groups of voxels segmented as air-filled pore space) are hereafter referred to as macropores. The total number of individual macropore clusters ($N_p$) per ROI was also calculated. Continuous macropores were defined as the macroporosity which is connected to both the top and bottom faces of the ROI. Voxels were connected if they shared a face (i.e., the 6 nearest neighbours in 3D). The connected macroporosity was calculated as the ratio of the number of voxels constituting the continuous macroporosity divided by the total number of voxels in the ROI.

## 2.3. Solute breakthrough test

After CT scanning, cavities on the bottom of the soil columns were filled with fine sand to create a planar surface. A polyamide textile cloth (50 μm mesh size) was tightened over the bottom of the column to keep the sand in place. The soil columns were then placed on a stainless steel flow collector. Effluent from the columns was conducted through flow cells where the electrical conductivity of the effluent was measured and logged at 1 min intervals using electrical conductivity meters (Cond 3310, WTW GmbH, Weilheim, Germany).

The soil columns were first irrigated with tap water with a background electrical conductivity of 470 μS cm$^{-1}$ at a constant rate, 5 mm h$^{-1}$, in a laboratory irrigation chamber (Liu et al., 2012) with free drainage at the base, until steady-state conditions were established. This flow rate is not unrealistically high for field conditions in Sweden and should be sufficiently large to generate flow in macropores in this kind of clay soil with low matrix hydraulic conductivity (Jarvis, 2007). For the columns sampled from the Upper site, a Dirac-like pulse of potassium bromide solution (electrical conductivity of 46,700 μS cm$^{-1}$) was applied at

the soil surface while the steady-state irrigation of 5 mm h$^{-1}$ was maintained. The experiment was continued until the electrical conductivity in the effluent approached the background value. Many of the samples from the Lower site exhibited very low hydraulic conductivities which made it impossible to carry out the solute breakthrough test with this method (see Table 2). The solute breakthrough experiments on the columns from the Lower site were therefore carried out under ponding conditions. After slowly saturating the columns from the base, 20 cm of tap water was ponded at the soil surface in order to flush out resident solutes from the soil. After the height of ponded water had receded below 5 cm, the remaining water was siphoned off until it was less than 0.5 cm. 20 cm of tracer solution was then added (1778 to 2130 μS cm$^{-1}$) and allowed to infiltrate, resulting in solute breakthrough curves (BTCs) covering approximately two pore-volumes. The non-steady infiltration rate was measured throughout these experiments.

The BTCs were standardized such that the relative electrical conductivity in the effluent, $C$ (−) (i.e., outflow electrical conductivity at a given time divided by the inflow conductivity) was used as a proxy for the bromide concentration and the cumulative outflow, $\eta$ (cm), as a proxy for time. It is known that the relationship between solute concentration and electrical conductivity is approximately linear for the low solute concentrations used in our study (Silbey and Alberty, 2000). For simplicity, we assumed a perfectly linear relationship between changes in electrical conductivity and changes in bromide concentration therefore directly addressed the electrical conductivity BTCs as bromide BTCs.

We analyzed the breakthrough curves using non-parametric shape-measures (Koestel et al., 2011). This requires that the shape of the transfer-function associated to the BTC is preserved as good as possible during the de-convolution of the breakthrough curve. A mix of two log-normal probability density functions, $f$ (cm$^{-1}$), serves this purpose (Koestel et al., 2011) and was subsequently used for BTC de-convolution interpolation between individual measurements:

**Table 2**
Pore characteristics, $K_a$, $K_s$ and $t_{0.05}$ for the Lower site.

| Lower site | Plot number | Sample | Macroporosity (%) | Connected porosity (%) | $N_P$ | $K_a$ (μm$^2$) | $K_s$ (cm h$^{-1}$) | $t_{0.05}$ (−) |
|---|---|---|---|---|---|---|---|---|
| Trafficked | 1 | 1 | 0.1 | 0 | 288 | 1 | 0.03 | 0.25 |
| | 1 | 2 | 0.06 | 0.01 | 229 | 6.1 | 0.08 | 0.15 |
| | 2 | 1 | 0.12 | 0 | 397 | 0.1 | [a] | 0.27 |
| | 2 | 2 | 0.06 | 0 | 166 | 17.2 | 0.06 | 0.25 |
| | 3 | 1 | 0.18 | 0 | 351 | 1.6 | 0.02 | 0.3 |
| | 3 | 2 | 0.12 | 0 | 345 | 0.5 | 0.38 | 0.19 |
| | 4 | 1 | 0.06 | 0 | 362 | 3 | 0.02 | 0.37 |
| | 4 | 2 | 0.06 | 0 | 284 | 2.4 | 0.06 | |
| Mean | | | 0.09 | 0.001 | 302.8 | 4.0 | 0.09 | 0.25 |
| Std. Dev. | | | 0.05 | 0.003 | 76.7 | 5.7 | 0.13 | 0.07 |
| Control | 1 | 1 | 0.17 | 0.01 | 406 | 6.1 | 0.04 | 0.05 |
| | 1 | 2 | 0.18 | 0 | 354 | 1.2 | 0.08 | 0.12 |
| | 2 | 1 | 0.12 | 0 | 397 | 13.2 | 25.2 | 0.22 |
| | 2 | 2 | 0.31 | 0.02 | 633 | 28.4 | 35.6 | 0.07 |
| | 3 | 1 | 0.11 | 0 | 464 | 10.1 | 13.6 | 0.13 |
| | 3 | 2 | 0.06 | 0 | 347 | 15.2 | 0.07 | 0.12 |
| | 4 | 1 | 0.18 | 0.01 | 494 | 12.2 | 10 | 0.03 |
| | 4 | 2 | 0.14 | 0 | 494 | 10.1 | 2.9 | 0.31 |
| Mean | | | 0.16 | 0.005 | 448.6 | 12.1 | 10.9 | 0.13 |
| Std. Dev. | | | 0.07 | 0.007 | 94.2 | 7.9 | 13.3 | 0.09 |
| prob > |t| | | | 0.1 | 0.2 | 0.004 | 0.02[b] | 0.05[b] | 0.02 |

*Note:* $N_p$: number of pore clusters; $K_a$: air permeability; $K_s$: saturated hydraulic conductivity; $t_{0.05}$: 5% arrival-time.
[a] The column in block 2 of the trafficked plot at Lower site had a very low hydraulic conductivity which made it impossible to measure $K_s$ for this column under 5 mm h$^{-1}$ irrigation intensity.
[b] P values were calculated using log-transformed values for $K_a$ and $K_s$.

$$f(\eta) = \underbrace{\arg\min}_{\mu_{ln1}, \sigma_{ln1}, \mu_{ln2}, \sigma_{ln2}, k}$$

$$\sum_0^{\eta_e} \left[ C - \alpha(\eta) * \left\{ k f_{ln1}\left(\eta; \mu_{ln1}, \sigma_{ln1}\right) + (1-k) f_{ln2}\left(\eta; \mu_{ln2}, \sigma_{ln2}\right) \right\} \right]^2 \qquad (2)$$

where each of the two $f_{ln}$ functions take the form of

$$f_{ln}(\eta) = \frac{1}{[\sigma_{ln}\eta\sqrt{2\pi}]}\exp\left[ -\frac{\left(\ln(\eta) - \mu_{ln}\right)^2}{2\sigma_{ln}^2} \right] \qquad (3)$$

where $\mu_{ln}$ (dimensionless) is the mean of $\ln\eta$ and $\sigma_{ln}$ (dimensionless) is the standard deviation of $\ln\eta$, $\eta_e$ is the cumulative outflow at the end of each breakthrough experiment, $\kappa$ is a weighting factor and $\alpha$ (cm) is the Dirac delta function for the experiments at the Upper site and the Heaviside step function at the Lower site. The asterisk denotes the convolution operator. The probability density functions $f$ were then used to obtain the cumulative outflow, $\eta_{0.05}$ (cm), after which 5% of the applied bromide had arrived (Upper site) or after which the bromide concentration in the effluent had reached 5% of the applied bromide concentration (Lower site). We derived relative 5%-arrival 'times', $t_{0.05}$ ($-$) by dividing $\eta_{0.05}$ by $\mu_{ln}$. This non-parametric shape measure has been identified as a robust indicator of preferential transport (Ghafoor et al., 2013; Knudby and Carrera, 2005; Koestel et al., 2011). Smaller values of $t_{0.05}$ indicate stronger preferential flow.

### 2.4. Saturated hydraulic conductivity and air-permeability

The saturated hydraulic conductivity, $K_s$, of each column was measured using the falling-head method according to Jury et al. (1991), with an initial ponding height at the soil surface of 20 cm using the setup explained above for the BTC experiments on the columns from the Lower site. Air-permeability, $K_a$, has also been found to be a sensitive measure of soil structure and macropore networks (Tuli et al., 2005). $K_a$ was measured at the initial soil water content at the time of sampling using an air pressure gradient of 5 hPa according to the steady-state method described by Iversen et al. (2001). The volumetric air-flow rate through the soil columns was recorded and the air-permeability was then calculated from Darcy's law.

### 2.5. Statistical analysis

All statistical analyses were performed with the JMP Pro 11 software (SAS Institute Inc.). Significant differences between means were determined by Student's $t$-test and $p$-values less than 0.05 were considered statistically significant. Correlation and regression analyses were performed between measured parameters ($K_s$, $K_a$, macroporosity, connected porosity and $t_{0.05}$). Goodness-of-fit was assessed by the coefficient of determination ($R^2$) with $p$-values less than 0.05. The logarithms of $K_s$ and $K_a$ were used in all the statistical analyses, since the measured data covered more than two orders of magnitude and were not to be normally distributed according to Shapiro–Wilk normality test.

### 3. Results and discussion

#### 3.1. Macroporosity

The X-ray images shown in Fig. 1 give a visual impression of the macropore systems at both sites. As shown in Tables 2 and 3, macroporosity at the Upper site was larger than at the Lower site. The proportion of the imaged macroporosity connected from the top to the bottom of the column was generally small: only 12 of the 32 samples had macropores that were continuous across the column (8 at the Upper site and 4 at the Lower site; Tables 3 and 2). The connected porosity was also larger at the Upper site than at the Lower site.

Although there was a tendency for a smaller macroporosity and number of pores in the trafficked treatment compared with the control at the Upper site, these effects were not significant (Table 3). In contrast, compaction was found to significantly decrease the number of pores ($p = 0.004$) at the Lower site (Table 2), but not the macroporosity and the connected porosity. The reasons for the differences between the two sites in their response to compaction may be related to the different crops at the time of compaction (grass ley at the Upper site vs. cereal stubble at the Lower site) and differences in soil moisture conditions (the soil at the Upper site was drier).

#### 3.2. Saturated hydraulic conductivity and air permeability

Compaction was found to significantly ($p < 0.05$) decrease both $K_s$ (from a mean of 10.9 cm h$^{-1}$ to 0.1 cm h$^{-1}$) and $K_a$ (from a mean of 12.1 $\mu$m$^2$ to 4.0 $\mu$m$^2$) at the Lower site (Table 2), which is consistent with the reduced macroporosity and connected porosity. No significant effect of traffic compaction on $K_s$ and $K_a$ was found at the Upper site, which also is consistent with the measurements of total and connected macroporosity discussed above (Table 3). $K_s$ and $K_a$ were significantly correlated at both sites (Fig. 2), as can be expected from theoretical considerations (Ghanbarian et al., 2014). Since variation in the initial water content may have affected $K_a$, we focus on the measurements of $K_s$ in the remainder of this paper. $K_s$ is significantly correlated with macroporosity, decreasing rapidly as the imaged macroporosity decreases towards zero (Fig. 3a). A power law function gives a good fit to the relationship between $K_s$ and connected porosity (Fig. 3b). From Fig. 3b it is also evident that there is a large variation in $K_s$ (from 0.06 cm h$^{-1}$ to 34 cm h$^{-1}$) between the 20 columns with no connected imaged porosity. Macroporosity in these columns varied from 0.18% to 0.5% (Tables 2 and 3). So, in these columns, variation in $K_s$ depended on connected porosity below the resolution of the X-ray. Hence the significant effects of compaction on the flow properties of the soil at the Lower site partly resulted from effects on the volume, size distribution, tortuosity and continuity of pores smaller than the image resolution of 1.2 mm.

#### 3.3. Solute breakthrough curves

The 5% arrival time, $t_{0.05}$, was significantly larger in trafficked soil (mean of 0.25) at the Lower site than in the control (mean of 0.13), which means that compaction limited the strength of preferential flow in this soil (Table 2). Consistent with the other measurements, no significant effect of traffic on preferential flow was found at the Upper site (Table 3), although this may have been influenced by one outlier in the control, as $t_{0.05}$ values were generally larger in the trafficked treatment. An inverse relationship between $t_{0.05}$ and macroporosity was found at the Lower site,
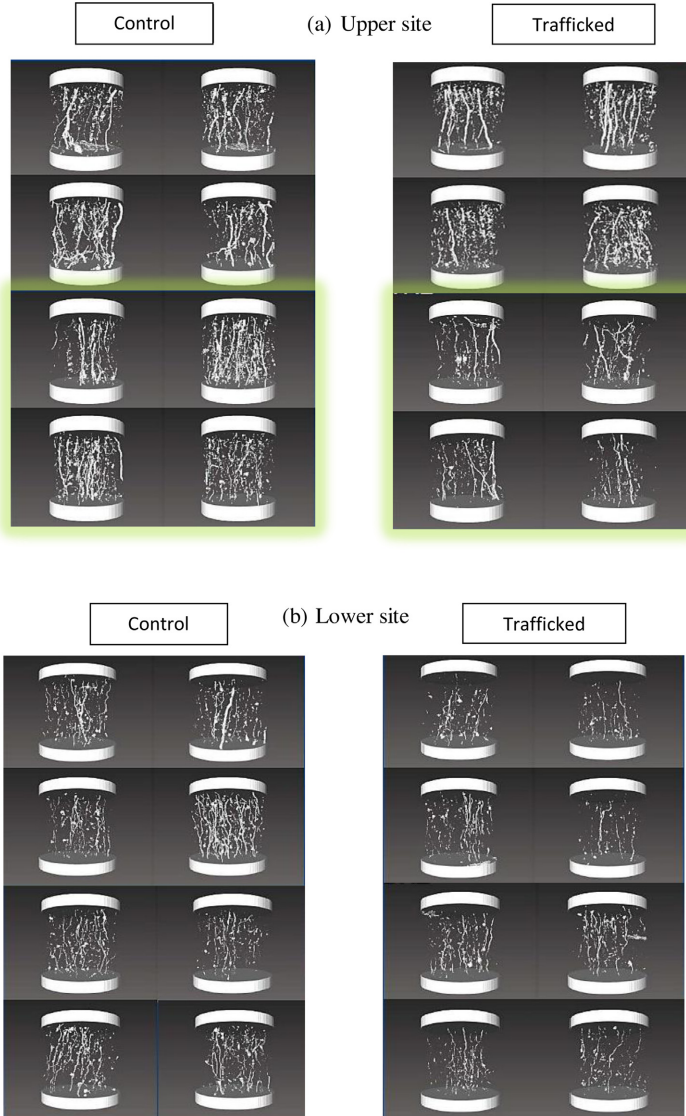
**Fig. 1.** Images of the macropore networks in the trafficked and control plots in upper site (a) and lower site (b).

whereas no trend was apparent at the Upper site (Fig. 4). A loss of macroporosity due to severe compaction may decrease preferential flow by reducing macropore continuity (Jarvis, 2007). The connected porosity in the soil of the control treatment at the Lower site was larger than in the trafficked soil, but not at a significant level. Following the same reasoning as for $K_s$, the effect of compaction on preferential flow may be attributed partly to a reduction in the volume and continuity of macropores that are smaller than the resolution of the X-ray scanner used in this study.

The trade-off between sample size and image resolution is a well-known limitation of the X-ray technique, although other CT-systems (e.g., industrial scanners) will give better resolution than the medical scanner used in this study.

In a meta-analysis carried out on 733 tracer BTC experiments, (Koestel et al., 2012) found an average $t_{0.05}$ of approximately 0.5 for sieved and repacked soil without macropores and an average $t_{0.05}$ of 0.22 for undisturbed soils. They then assumed that a $t_{0.05}$ of larger than 0.5 indicates absence of preferential flow, a

**Table 3**
Pore characteristics, $K_a$, $K_s$ and $t_{0.05}$ for the Upper site.

| Upper site | Plot number | Sample | Macroporosity (%) | Connected porosity (%) | $N_P$ | $K_a$ (µm$^2$) | $K_s$ (cm h$^{-1}$) | $t_{0.05}$ (−) |
|---|---|---|---|---|---|---|---|---|
| Trafficked | 1 | 1 | 0.54 | 0.25 | 613 | 83.0 | 97.0 | 0.10 |
| | 1 | 2 | 0.61 | 0.07 | 675 | 43.5 | 98.6 | 0.21 |
| | 2 | 1 | 0.37 | 0.00 | 813 | 7.1 | 2.6 | 0.16 |
| | 2 | 2 | 0.53 | 0.00 | 748 | 3.6 | 2.2 | 0.08 |
| | 3 | 1 | 0.24 | 0.02 | 342 | 3.2 | 10.0 | 0.16 |
| | 3 | 2 | 0.21 | 0.00 | 319 | 12.2 | 22.2 | 0.13 |
| | 4 | 1 | 0.23 | 0.05 | 370 | 13.2 | 21.5 | 0.18 |
| | 4 | 2 | 0.10 | 0.00 | 270 | 2.0 | 1.7 | 0.28 |
| Mean | | | 0.35 | 0.05 | 518.7 | 21.0 | 32.0 | 0.16 |
| Std. Dev. | | | 0.19 | 0.08 | 216.3 | 28.4 | 41.4 | 0.06 |
| Control | 1 | 1 | 0.52 | 0.13 | 606 | 48.7 | [a] | 0.47 |
| | 1 | 2 | 0.38 | 0.00 | 623 | 26.3 | 29.4 | 0.06 |
| | 2 | 1 | 0.70 | 0.04 | 606 | 27.3 | 28.8 | 0.14 |
| | 2 | 2 | 0.46 | 0.00 | 399 | 11.2 | 8.5 | 0.08 |
| | 3 | 1 | 0.27 | 0.06 | 382 | 30.4 | 84.0 | 0.07 |
| | 3 | 2 | 0.61 | 0.12 | 997 | 63.8 | 55.3 | 0.14 |
| | 4 | 1 | 0.50 | 0.00 | 802 | 35.4 | 34.0 | 0.07 |
| | 4 | 2 | 0.27 | 0.00 | 723 | 25.1 | 24.0 | 0.08 |
| Mean | | | 0.46 | 0.04 | 642.3 | 33.5 | 37.7 | 0.14 |
| Std. Dev. | | | 0.15 | 0.06 | 202.7 | 16.1 | 24.7 | 0.14 |
| prob > \|t\| | | | 0.28 | 0.89 | 0.37 | 0.14[b] | 0.28[b] | 0.66 |

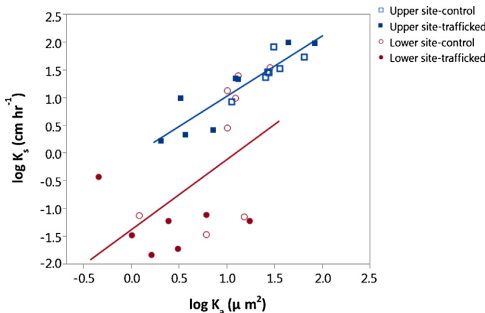Note: $N_p$: number of pore clusters; $K_a$: air permeability; $K_s$: saturated hydraulic conductivity; $t_{0.05}$: 5% arrival-time.
[a] The column in block 1 of the control plot at Upper site had a very fast flow which made it impossible to measure $K_s$ for this column. The reason was an earthworm channel passing through the entire column.
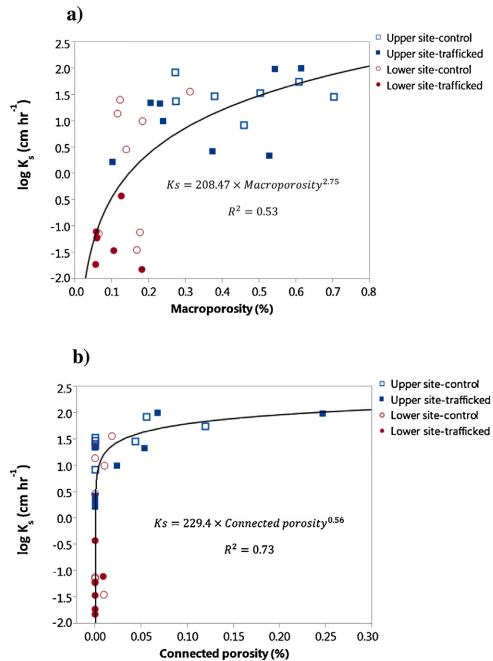[b] P values were calculated using log-transformed values for $K_a$ and $K_s$.

$t_{0.05}$ between 0.5 and 0.22 indicate weak, values around 0.22 normal and values smaller than 0.22 strong preferential flow. The $t_{0.05}$ values of both sites in this study were relatively small, indicating strong preferential transport, especially at the Upper site. It could be noted that the experiments at the Upper and Lower sites were carried out under different boundary conditions (near-saturated, flow-controlled vs. ponded), which should influence the $t_{0.05}$ values (Koestel et al., 2013; Larsbo et al., 2014). If the columns from the Upper site had been saturated, they would probably have shown even stronger preferential flow (i.e., smaller $t_{0.05}$ values).

At first glance, our results contrast markedly with those of Katuwal et al. (2015b), who found a strong positive correlation between $t_{0.05}$ and macroporosity derived by CT-scanning (with a similar image resolution) for 19 samples taken from an agricultural field in Denmark where the clay content varied from 14.7 to 18.2%.

a)

$Ks = 208.47 \times Macroporosity^{2.75}$

$R^2 = 0.53$

b)

$Ks = 229.4 \times Connected\ porosity^{0.56}$

$R^2 = 0.73$

**Fig. 3.** Relationship between $K_s$ and Macroporosity (a) and Connected porosity (b).

**Fig. 2.** Relationship between $K_a$ (air permeability) and $K_s$ (saturated hydraulic conductivity) of each site (upper site and lower site);
log $K_s$ (Upper site) = −0.04 + 1.09 × log $K_a$; $R^2$ (Upper site) = 0.82; $P$ = 0.03
log $K_s$ (Lower site) = −1.36 + 1.26 × log $K_a$; $R^2$ (Lower site) = 0.30; $P$ = 0.0001
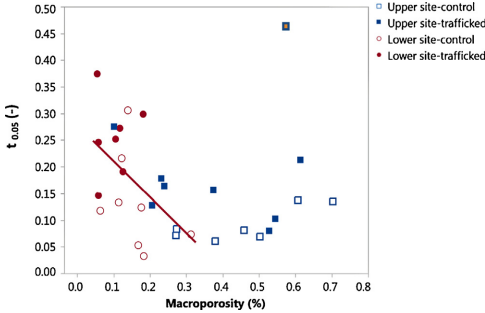
**Fig. 4.** Relationship between $t_{0.05}$ (5% arrival time) and Macroporosity. The $t_{0.05}$ in a control plot at Upper site (the orange square mark) was considered as outlier. The reason was because earthworm channel passing through the entire column which caused a very fast flow.
$t_{0.05}$ (Lower site) $= 0.3 - 0.67 \times$ Macroporosity; $R^2 = 0.2$; $P = 0.09$

However, their samples all had macroporosities larger than ca. 0.4%, while most of our columns had much smaller values (Tables 2 and 3), and soil texture was quite different. Larsbo et al. (2014) also found a greater degree of preferential flow (i.e., smaller $t_{0.05}$ values) in topsoil samples with smaller saturated hydraulic conductivities and X-ray imaged macroporosities. In marked contrast to the columns in our study, macroporosities in these recently tilled soils were large (varying between ca. 3 and 10%) and Larsbo et al. (2014) found that the continuity of the macropore networks was maintained across the samples in all but 2 of their 18 columns. Thus, taken together, these studies suggest that, as hypothesized by Jarvis (2007), moderate compaction should increase the strength of preferential flow as macroporosity decreases but few continuous macropores remain. As demonstrated by Ghafoor et al. (2013) and Larsbo et al. (2014), this is due to a decrease in the hydraulic conductivity near saturation, which means that larger remaining pores will conduct the flow. As compaction becomes more severe, a critical point is reached at which pore continuity limits preferential flow. At this point, the saturated hydraulic conductivity of the soil may become so small, that surface runoff may occur depending on the surface boundary conditions in the field. This reasoning is summarized in the conceptual model presented in Fig. 5a and b, which illustrates how preferential flow and surface runoff may be affected by compaction events and the natural re-generation of soil structural macropores (e.g., due to cracking or earthworm activity) following compaction. Moderate compaction may induce stronger preferential flow due to a decrease in near-saturated hydraulic conductivity and increase in the size of the largest conducting (i.e., water-filled) pore (compare curve B to curve A in Fig. 5a), while more severe compaction results in an increased risk of surface runoff and weaker preferential flow, since the size of the largest pore in the soil is dramatically decreased (curve C). Larger soil macropores such as cracks and earthworm channels may subsequently regenerate, while the recovery of smaller pores affected by compaction is a slower process. This may lead to very strong preferential flow (curve D).
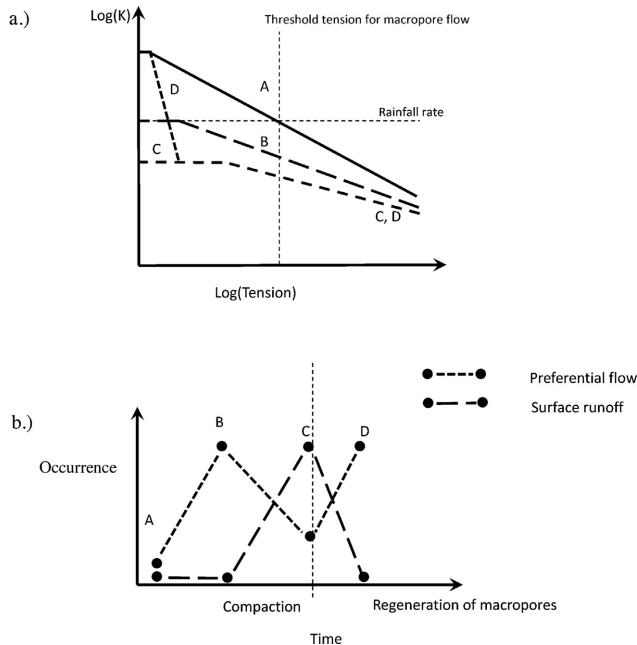


**Fig. 5.** Conceptual model of preferential flow as influenced by soil compaction and subsequent recovery from compaction. (a) Near saturated hydraulic conductivity as a function of soil water tension, (b) The time-dependence of preferential flow and runoff as a function of compaction and recovery from compaction; A: no compaction, B: moderate compaction, C: strong compaction, D: regeneration of macropores after compaction.

## 4. Conclusions

At one site, no compaction resulted from the traffic treatment. At the second site with the smallest initial macroporosity and saturated hydraulic conductivity, the soil was compacted by the traffic treatment, as shown by a significant reduction in saturated hydraulic conductivity, air permeability and the number of macropores. At this site, the traffic compaction also significantly reduced the strength of preferential flow. The significant effects of compaction on the flow and transport properties mostly resulted from effects on the volume and continuity of pores smaller than 1.2 mm, which was the resolution of the X-ray imaging in our study.

Our results are in apparent contrast with those obtained in some previous studies in which preferential flow has been shown to increase following compaction. These contradictions were explained with the help of a conceptual model, which suggests that preferential flow should be strongest at some intermediate level of compaction, at which macropore continuity is still maintained despite reductions in macroporosity. This model also illustrates how compaction and subsequent recovery from compaction should affect susceptibility to preferential flow and surface runoff.

## References

Alaoui, A., Goetz, B., 2008. Dye tracer and infiltration experiments to investigate macropore flow. Geoderma 144, 279–286.

Allaire, S.E., Roulier, S., Cessna, A.J., 2009. Quantifying preferential flow in soils: a review of different techniques. J. Hydrol. 378, 179–204.

Arvidsson, J., 1997. Soil Compaction in Agriculture—from Soil Stress to Plant Stress. Swedish Univ. of Agricultural Sciences, Agraria, pp. 41.

Arvidsson, J., Håkansson, I., 1996. Do effects of soil compaction persist after ploughing? Results from 21 long-term field experiments in Sweden. Soil Till. Res. 39, 175–197.

Coquet, Y., Coutadeur, C., Labat, C., Vachier, P., van Genuchten, T., Roger-Estrade, J., Simunek, J., 2005. Water and solute transport in a cultivated silt loam soil: 1. Field observations. Vadose Zone J. 4, 573–586.

Etana, A., Håkansson, I., 1994. Swedish experiments on the persistence of subsoil compaction caused by vehicles with high axle load. Soil Till. Res. 29, 167–172.

Etana, A., Larsbo, M., Keller, T., Arvidsson, J., Schjønning, P., Forkman, J., Jarvis, N., 2013. Persistent subsoil compavtion and its effects on preferential flow patterns in a loamy till soil. Geoderma 192, 430–436.

Ghafoor, A., Jarvis, N.J., Stenström, J., 2013. Modelling pesticide sorption in the surface and subsurface soils of an agricultural catchment. Pest Manag. Sci. 69, 919–929.

Ghanbarian, B., Hunt, A.G., Ewing, R.P., Skinner, T.E., 2014. Theoretical relationship between saturated hydraulic conductivity and air permeability under dry conditions: continuum percolation theory. Vadose Zone J. 13.

Heitman, J.L., Gaur, A., Horton, R., Jaynes, D.B., Kaspar, T.C., 2007. Field measurement of soil surface chemical transport properties for comparison of management zones. Soil Sci. Soc. Am. J. 71, 529–536.

Hendrickx, J.M.H., Flury, M., 2001. Uniform and preferential flow mechanisms in the vadose zone. Conceptual Models of Flow and Transport in the Fractured Vadose Zone. National Academy Press, Washington, D.C, pp. 149–187.

Iversen, B.V., Moldrup, P., Schjønning, P., Loll, P., 2001. Air and water permeability in differently textured soils at two measurement scales. Soil Sci. 166, 643–659.

Janssen, M., Lennartz, B., 2008. Characterization of preferential flow pathways through paddy bunds with dye tracer tests. Soil Sci. Soc. Am. J. 72, 1756–1766.

Jarvis, N.J., 2007. A review of non-equilibrium water flow and solute transport in soil macropores: principles, controlling factors and consequences for water quality. Eur. J. Soil Sci. 58, 523–546.

Jury, W.A., Gardner, W.R., Gardner, W.H., 1991. Water movement in soil, Soil Physics. fifth ed. John Willey & Sons, New York, pp. 73–121.

Katuwal, S., Moldrup, P., Lamandé, M., Tuller, M., de Jonge, L.W., 2015a. Effects of CT number derived matrix density on preferential flow and transport in a macroporous agricultural soil. Vadose Zone J. 14 doi:http://dx.doi.org/10.2136/vzj2015.01.0002.

Katuwal, S., Norgaard, T., Moldrup, P., Lamande, M., Wildenschild, D., de Jonge, L.W., 2015b. Linking air and water transport in intact soils to macropore characteristics inferred from X-ray computed tomography. Geoderma 237, 9–20.

Koestel, J.K., Norgaard, T., Luong, N.M., Vendelboe, A.L., Moldrup, P., Jarvis, N.J., et al., 2013. Links between soil properties and steady-state solute transport through cultivated topsoil at the field scale. Water Resour. Res. 49, 790–807. doi:http://dx.doi.org/10.1002/wrcr.20079.

Kim, H., Anderson, S.H., Motavalli, P.P., Gantzer, C.J., 2010. Compaction effects on soil macropore geometry and related parameters for an arable field. Geoderma 160, 244–251.

Knudby, C., Carrera, J., 2005. On the relationship between indicators of geostatistical, flow and transport connectivity. Adv. Water Resour. 28, 405–421.

Koestel, J.K., Moeys, J., Jarvis, N.J., 2011. Evaluation of nonparametric shape measures for solute breakthrough curves. Vadose Zone J. 10, 1261–1275.

Koestel, J.K., Moeys, J., Jarvis, N.J., 2012. Meta-analysis of the effects of soil properties, site factors and experimental conditions on solute transport. Hydrol. Earth Syst. Sci. 16, 1647–1665.

Kulli, B., Gysi, M., Flühler, H., 2003. Visualizing soil compaction based on flow pattern analysis. Soil Till. Res. 70, 29–40.

Lamandé, M., Wildenschild, D., Berisso, F.E., Garbout, A., Marsh, M., Moldrup, P., Keller, T., Hansen, S.B., de Jonge, L.W., Schjønning, P., 2013. X-ray CT and laboratory measurements on glacial till subsoil cores: assessment of inherent and compaction-affected soil structure characteristics. Soil Sci. 178, 359–368.

Larsbo, M., Koestel, J., Jarvis, N., 2014. Relations between macropore network characteristics and the degree of preferential solute transport. Hydrol. Earth Syst. 18, 5255–5269.

Lipiec, J., Hatano, R., 2003. Quantification of compaction effects on soil physical properties and crop growth. Geoderma 116, 107–136.

Lipiec, J., Wojciga, A., Horn, R., 2009. Hydraulic properties of soil aggregates as influenced by compaction. Soil Till. Res. 103, 170–177.

Liu, J., Aronsson, H., Ulén, B., Bergström, L., 2012. Potential phosphorus leaching from sandy topsoils with different fertilizer histories before and after application of pig slurry. Soil Use Manag. 28, 457–467.

Mooney, S.J., Nipattasuk, W., 2003. Quantification of the effects of soil compaction on water flow using dye tracers and image analysis. Soil Use Manag. 19, 356–363.

Pires, L.F., 2011. Gamma-ray computed tomography to evaluate changes in the structure of a clayey soil due to agricultural traffic. Acta Sci. Agron. 33, 411–416.

Richard, G., Cousin, I., Sillon, J.F., Bruand, A., Guerif, J., 2001. Effect of compaction on the porosity of a silty soil: influence on unsaturated hydraulic properties. Eur. J. Soil Sci. 52, 49–58.

Schjønning, P., Lamandé, M., Berisso, F.E., Simojoki, A., Alakukku, L., Andreasen, R.R., 2013. Gas diffusion, non-darcy air permeability, and computed tomography images of a clay subsoil affected by compaction. Soil Sci. Soc. Am. J. 77, 1977–1990.

Schulte, E.E., Hopkins, B.G., 1996. Estimation of Soil Organic Matter by Weight Loss-on-ignition. SSSA Special Publication, pp. 21–31.

Schwen, A., Lawrence-Smith, G.H.–R.–E.J., Sinton, S.M., Carrick, S., Clothier, B.E., Buchan, G.D., Loiskandl, W., 2011. Hydraulic properties and the water-conducting porosity as affected by subsurface compaction using tension infiltrometers. Soil Sci. Soc. Am. J. 75, 822–831.

Servadio, P., Marsili, A., Pagliai, M., Pellegrini, S., Vignozzi, N., 2001. Effects on some clay soil qualities following the passage of rubber-tracked and wheeled tractors in central Italy. Soil Till. Res. 61, 143–155.

Silbey, R.J., Alberty, R.A., 2000. Physical Chemistry, 3rd ed. John Wiley & Sons.

Soares, A., Moldrup, P., Vendelboe, A.L., Katuwal, S., Norgaard, T., Delerue-Matos, C., Tuller, M., De Jonge, L.W., 2015. Effects of soil compaction and organic carbon content on preferential flow in loamy field soils. Soil Sci. 180, 10–20.

Tuli, A., Hopmans, J.W., Rolston, D.E., Moldrup, P., 2005. Comparison of air and water permeability between disturbed and undisturbed soils. Soil Sci. Soc. Am. J. 69, 1361–1371.

II

WILEY SoilUse and Management

# Effects of compaction on soil hydraulic properties, penetration resistance and water flow patterns at the soil profile scale

**Mona Mossadeghi-Björklund[1]** [iD] | **Nicholas Jarvis[1]** [iD] | **Mats Larsbo[1]** [iD] |
**Johannes Forkman[2]** [iD] | **Thomas Keller[1,3]** [iD]

[1]Department of Soil and Environment, Swedish University of Agricultural Sciences, Uppsala, Sweden

[2]Department of Crop Production Ecology, Swedish University of Agricultural Sciences, Uppsala, Sweden

[3]Department of Agroecology and Environment, Agroscope, Zürich, Switzerland

**Correspondence**
Mona Mossadeghi-Björklund, Department of Soil and Environment, Swedish University of Agricultural Sciences, Uppsala, Sweden.
Email: mmossadeghi@gmail.com

**Abstract**

The aim of this study was to quantify the effects of compaction on water flow patterns at the soil profile scale. Control and trafficked plots were established in field trials at two sites. The trafficked treatment was created by four passes track-by-track with a three-axle dumper with a maximum wheel load of 5.8 Mg. One year later, dye-tracing experiments were performed and several soil mechanical, physical and hydraulic properties were measured to help explain the dye patterns. Penetration resistance was measured to 50 cm depth, with saturated hydraulic conductivity ($K_s$), bulk density, and macroporosity and mesoporosity being measured on undisturbed soil cores sampled from three depths (10, 30 and 50 cm). Significant effects of the traffic treatment on the structural pore space were found at 30 cm depth for large mesopores (0.3–0.06 mm diameter), but not small mesopores (0.06–0.03 mm) or macroporosity (pores > 0.3 mm). At one of the sites, ponding was observed during the dye-tracing experiments, especially in the trafficked plots, because of the presence of a compacted layer at plough depth characterized by a larger bulk density and smaller structural porosity and $K_s$ values. Ponding did not induce any preferential transport of the dye solution into the subsoil at this site. In contrast, despite the presence of a compacted layer at 25–30 cm depth, a better developed structural porosity in the subsoil was noted at the other site which allowed preferential flow to reach to at least 1 m depth in both treatments.

**KEYWORDS**

dye tracing, macroporosity, penetrometer resistance, saturated hydraulic conductivity, soil compaction

# 1 | INTRODUCTION

Soil compaction is the process by which bulk density increases and porosity decreases owing to natural processes or under the action of an externally applied stress such as wheel trafficking. Larger pores in soil are known to be most susceptible to compaction, which can therefore potentially impose severe limitations on infiltration and water flow (e.g., Alaoui, Rogger, Peth, & Blöschl, 2018; Håkansson & Lipiec, 2000). Compaction may, however, lead to fast (preferential) water flow through any vertically oriented macropores, such as earthworm burrows and root channels that survive compaction. This may significantly impact groundwater quality (Jarvis, 2007). Quantifying long-term effects of soil compaction on water flow patterns is challenging, not least because of the interplay between field traffic-induced compaction and the natural recovery processes (both physical and biological) following compaction that affect soil structure. This

complexity means that the impacts of compaction on water flow patterns in agricultural soils are still poorly understood (Rogger et al., 2017).

Dye tracing has proven useful as a method to visualize and quantify compaction effects on flow patterns at the soil profile scale (e.g., Alaoui & Goetz, 2008; Etana et al., 2013; Kulli, Gysi, & Flühler, 2003). However, the method is very time-consuming which means that the number of replicates that can be obtained is limited. This means that statistically significant differences between treatments may not be easy to establish because of the often observed large spatial variation in soil properties (Jarvis, Koestel, & Larsbo, 2016). Combining dye staining experiments with easy-to-measure, in situ soil profile scale measurements of relevant mechanical, physical and hydraulic properties should therefore help to interpret changes in water flow patterns resulting from traffic compaction, leading to an improved understanding of the complex interplay between soil management, soil structure and function. The objective of our study was to investigate the effects of compaction on water flow patterns at the soil profile scale 1 year after wheeling, by combining dye tracing with penetrometer resistance measured in the field and bulk density, saturated hydraulic conductivity and water retention measured in the laboratory.

## 2 | MATERIALS AND METHODS

### 2.1 | Site description, experimental design and sampling

Compaction experiments were carried out on a clay soil at two nearby sites (hereafter denoted the "Upper site" and the "Lower site") close to Uppsala (59°48′N, 17°39′E), in central Sweden. The two sites were situated approximately 300 m apart. At the time of the sampling, the groundwater was located at ca. 1.2 m depth at the Upper site and approximately 50 cm higher at the Lower site. Table 1 gives basic data on soil texture and organic matter content at the two sites. More detailed site information can be found in Mossadeghi-Björklund et al. (2016). The experiment was designed as two randomized complete block trials with two treatments (trafficked and control), with four blocks at each

site and a plot size of 9 × 20 m. The trafficked treatment was created in November 2010, when the soil water content was close to field capacity, by four passes track-by-track with a three-axle dumper truck (Bell B25D 6 × 6) with 5.8, 5.4 and 4.6 Mg wheel load on the first, second and third axle and 420 kPa tyre inflation pressure (tyre size: 23.5R25). The Upper site was under grass ley at the time of compaction, while the surface of the Lower site was covered with cereal stubble following the harvest of the previous crop. After wheeling, both sites were mouldboard ploughed to a depth of approximately 20 cm. In 2011, oat was grown at both sites, with seedbed preparation and sowing in spring and harvest at the end of August. Soil core sampling and field measurements were then carried out in September 2011 almost 1 year after the wheeling treatment was applied, when the soil was slightly wetter than field capacity.

### 2.2 | Bulk density, saturated hydraulic conductivity and soil water retention

Undisturbed soil cores (5 cm height and 7.2 cm diameter) were sampled at both sites and in all plots at three depths (10, 30 and 50 cm) to measure soil water retention, saturated hydraulic conductivity and bulk density. In each plot, four samples were taken at 30 and 50 cm depth, and six samples at 10 cm depth. This amounted to a total of 288 samples. After sampling, the cores were gradually saturated from the bottom using tap water. Half of the samples (144) were randomly chosen for measurements of saturated hydraulic conductivity, $K_s$, using the constant-head method. The other half were used to measure bulk density and water retention at four different tensions, namely 10, 30, 50 and 100 hPa, using the sand-box method (Eijkelkamp, model 08.01). Finally, the samples were oven-dried, and the bulk density and volumetric water contents at each tension step were calculated. In the remainder of this paper, we use the term "macropores" to denote pores that drained between saturation and 10 hPa, "large mesopores" for those that emptied between 10 and 50 hPa and "small mesopores" for the volume of pores emptying between 50 and 100 hPa. Applying the Young-Laplace capillarity equation, these pressure potentials correspond to equivalent pore diameters of >0.3 mm

**TABLE 1** Soil texture and organic matter content of Upper site and Lower site

| Site | Depths | Clay % (<0.002 mm) | Silt % (0.002–0.06 mm) | Sand % (0.06–2 mm) | Organic matter (%) |
|------|--------|--------------------|-----------------------|--------------------|--------------------|
| Upper site | 15 cm | 47.3 | 31.5 | 21.2 | 3.5 |
| | 30 cm | 46.5 | 32 | 21.5 | 1.3 |
| | 50 cm | 46.5 | 35.3 | 18.2 | 0.3 |
| Lower site | 15 cm | 50 | 30 | 20 | 3 |
| | 30 cm | 50.5 | 32.5 | 17 | 0.3 |
| | 50 cm | 53.8 | 32.5 | 13.7 | 0 |
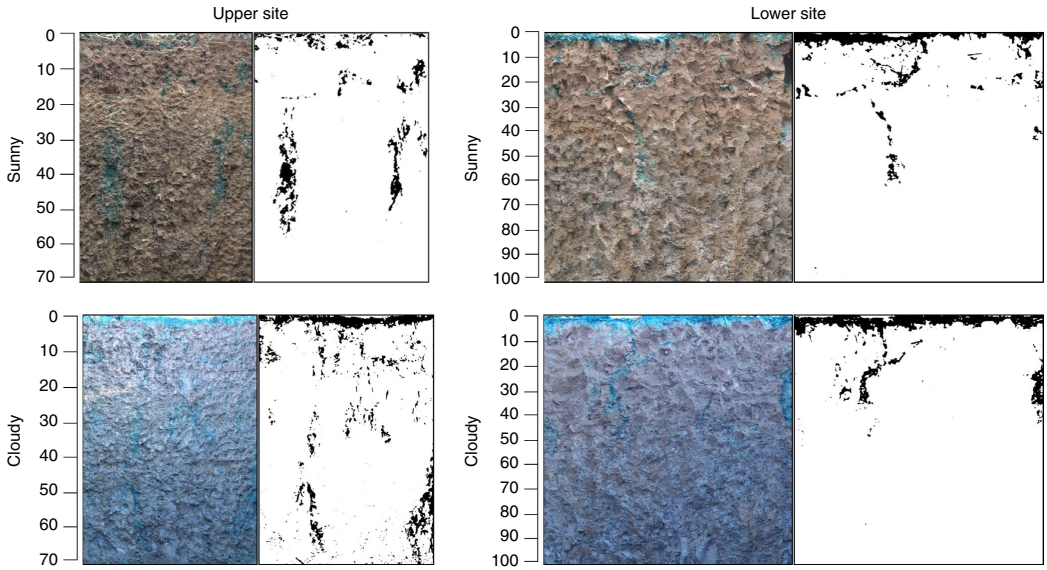
**FIGURE 1** Examples of dye-tracing images used for analysis of flow patterns at two sites and under different light conditions (sunny vs. cloudy)
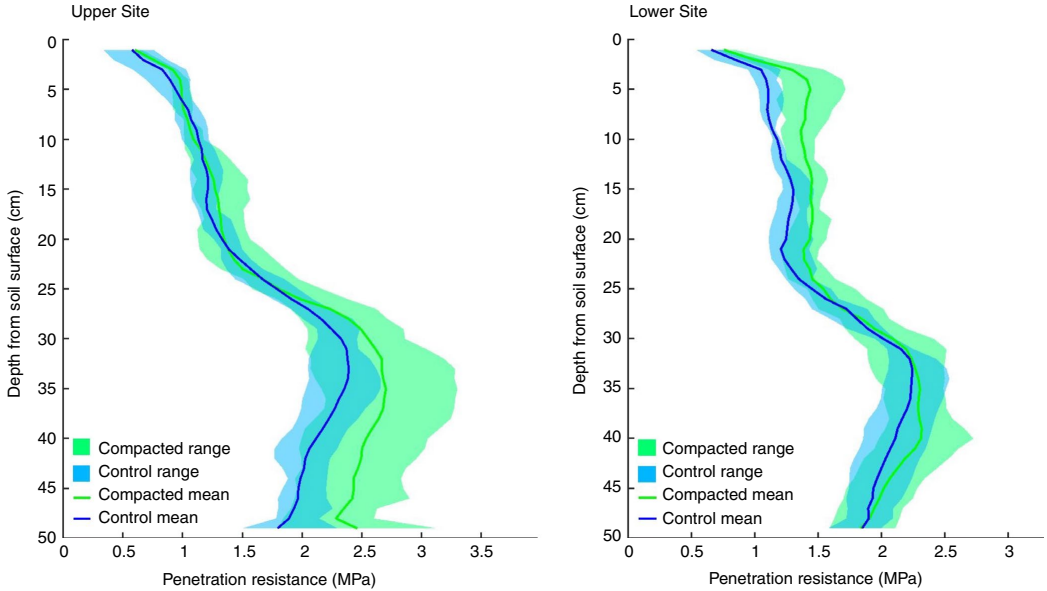


**FIGURE 2** Penetration resistance patterns at Upper site and Lower site before and after compaction

**T A B L E 2** Effects of soil depth on pore classes, saturated hydraulic conductivity ($K_s$) and bulk density (Bd)

| Depth (cm) | Porosity ≥0.03 mm ($m^3\ m^{-3}$) | Macropores ≥ 0.3 mm ($m^3\ m^3$) | Large mesopores 0.3–0.06 mm ($m^3\ m^{-3}$) | Small mesopores 0.06–0.03 mm ($m^3\ m^{-3}$) | $K_s$ (cm $hr^{-1}$) | Bd (g $cm^{-3}$) |
|---|---|---|---|---|---|---|
| 10 | 0.05 | 0.02 | 0.02 | 0.007 | 1.02 | 1.27 |
| 30 | 0.04 | 0.01 | 0.02 | 0.008 | 0.62 | 1.38 |
| 50 | 0.08 | 0.04 | 0.03 | 0.009 | 4.27 | 1.26 |
| $p$ Value (Depth) | 0.0006* | 0.02* | 0.0003* | 0.11 | 0.0005* | <0.0001* |
| SED | 0.009 | 0.008 | 0.003 | – | 0.19[a] | 0.02 |
| LSD | 0.02 | 0.02 | 0.007 | – | 0.39[a] | 0.035 |

*Notes.* [a]SED and LSD values for $K_s$ are in $log_{10}$ scale. *$p < 0.05$.

(macropores), 0.3–0.06 mm (large mesopores) and 0.06–0.03 mm (small mesopores).

## 2.3 | Penetrometer resistance

Soil penetration resistance was measured using a hand-held Eijkelkamp penetrologger with a cone of 1 $cm^2$ base area and 60° apex angle. Measurements were made to 50 cm depth at 15 randomly selected locations per plot.

## 2.4 | Dye tracing

A 1 $m^2$ area on each plot was irrigated with 20 L of water using a watering can. The irrigation was done at a different location than the core sampling. Twenty-four hours later, 30 L (=30 mm) of Brilliant Blue solution (4 g $L^{-1}$) was applied on the same areas. The solution was applied over 30 min at the Upper site. At the Lower site, where conditions were wetter, the Brilliant Blue solution was applied intermittently during a 4-hr period to avoid surface runoff as the soil surface started to pond. Twenty-four hours after the Brilliant Blue application, three vertical soil profiles for each plot were excavated to a depth of 150 cm, and then, the profile walls were carefully prepared with knives. The profiles were located 25, 35 and 45 cm into the dye-stained area.

Photographs were taken with a digital camera (Nikon R90) under the prevailing conditions, which included both sunny and cloudy weather. At the Upper site, photographs taken from the soil surface down to 100 cm were analysed, whereas this was only done to 70 cm depth at the Lower site because of differences in groundwater levels at the two sites. At the Upper site, blocks I and II were photographed under sunny conditions and blocks III and IV under cloudy conditions. At the Lower site, all photographs from blocks I and IV were taken under cloudy conditions while the photographs from block II were taken under sunny conditions. For block III, two photographs (one for each treatment) were taken under sunny conditions and four photographs under cloudy conditions.

## 2.5 | Image processing

Image processing was carried out using the Fiji distribution (Schindelin et al., 2012) of the software ImageJ (Abramoff, Magalhaes, & Ram, 2004). The images were first converted from the RGB colour space into the hue (H), saturation (S) and value (V) colour space where V represents the brightness of a pixel. The H, S and V values of photographs taken during sunny conditions differed significantly from those taken during cloudy conditions (Figure 1). These differences could not be corrected. We therefore divided the photographs into two groups and treated photographs taken during sunny and cloudy conditions separately. Within these groups, we assumed that differences in illumination only affected the V value. Hence, the HSV images were segmented to binary images using the same thresholds for H and S for all images within a group. We assigned different threshold values for the two sites and for the topsoil (0–25 cm depth) and the subsoil, since the colour of a soil is influenced by soil texture and organic matter content (Forrer, Papritz, Kasteel, Flühler, & Luca, 2000). All threshold values were determined by visual comparison of original images with the resulting binary images. Finally, a median filter was used to reduce noise in the binary images. The quantified dye patterns are to some extent subjective, as the binary images are influenced by the subjective choice of threshold values. However, it is still possible to evaluate differences between treatments, because the same operator analysed all images within a group using the same methods.

The soil profiles were divided into 2.5 cm thick horizontal layers. For each layer, we calculated two measures to characterize the dye staining patterns as follows: (a) the fraction of the area that was stained and (b) the average number of vertical flow paths. These calculations were carried out in Matlab version R2013b (8.2.0.701).

## 2.6 | Statistical analysis

Mixed-effects models were fitted to the data using JMP pro-11 statistical software. In these analyses, mean values per plot and depth were used as observations. The model comprised fixed effects of treatments, sites, depths, fixed effects

**TABLE 3** Comparisons between (1) Upper site and Lower site (2) Control and Trafficked treatments and effects of soil depth for pore classes (macropores, large mesopores and small mesopores), saturated hydraulic conductivity ($K_s$) and bulk density (Bd)

| Type | Depth (cm) | Porosity ≥0.03 mm (m³ m⁻³) | | | Macropores ≥0.3 mm (m³ m⁻³) | | | Large mesopores 0.3–0.06 mm (m³ m⁻³) | | | Small mesopores 0.06–0.03 mm (m³ m⁻³) | | | $K_s$ (cm h⁻¹) | | | Bd (g cm⁻³) | | |
|---|---|---|---|---|---|---|---|---|---|---|---|---|---|---|---|---|---|---|---|
| | | Upper | Lower | *p* | Upper | Lower | *p* | Upper | Lower | *p* | Upper | Lower | *p* | Upper | Lower | *p* | Upper | Lower | *p* |
| (1)[a] | 10 | 0.07 | 0.02 | 0.007* | 0.04 | 0.003 | 0.01* | 0.02 | 0.01 | 0.04* | 0.005 | 0.01 | 0.03* | 2.57 | 0.5 | 0.1 | 1.23 | 1.31 | 0.008* |
| | 30 | 0.06 | 0.01 | 0.004* | 0.03 | 0 | 0.01* | 0.02 | 0.01 | 0.04* | 0.01 | 0.005 | 0.02* | 2.09 | 0.22 | 0.04* | 1.35 | 1.41 | 0.02* |
| | 50 | 0.12 | 0.03 | 0.0002* | 0.06 | 0.01 | 0.001* | 0.05 | 0.02 | 0.005* | 0.01 | 0.006 | 0.02* | 11.75 | 1.58 | 0.02* | 1.19 | 1.32 | 0.0001* |
| | SED | 0.013 | 0.012 | | – | – | | 0.005 | – | | – | – | | 0.276[c] | 0.26[c] | | 0.024 | 0.023 | |
| | LSD | 0.027 | 0.025 | | – | – | | 0.010 | – | | – | – | | 0.574[c] | 0.54[c] | | 0.050 | 0.048 | |
| | *p* | 0.0003* | 0.0006* | | 0.053 | 0.31 | | <0.0001* | 0.49 | | 0.09 | 0.74 | | 0.01* | 0.009* | | <0.0001* | 0.0003* | |
| | | Control | Traffic | *p* | Control | Traffic | *p* | Control | Traffic | *p* | Control | Traffic | *p* | Control | Traffic | *p* | Control | Traffic | *p* |
| (2)[b] | 10 | 0.06 | 0.04 | 0.09 | 0.03 | 0.02 | 0.26 | 0.02 | 0.02 | 0.26 | 0.008 | 0.009 | 0.73 | 0.56 | 2.3 | 0.008* | 1.24 | 1.3 | 0.03* |
| | 30 | 0.05 | 0.03 | 0.12 | 0.02 | 0.006 | 0.24 | 0.02 | 0.01 | 0.02* | 0.01 | 0.01 | 0.6 | 1.55 | 0.3 | 0.01* | 1.34 | 1.42 | 0.04* |
| | 50 | 0.07 | 0.08 | 0.47 | 0.03 | 0.04 | 0.65 | 0.03 | 0.03 | 0.3 | 0.008 | 0.01 | 0.36 | 3.16 | 5.75 | 0.38 | 1.27 | 1.24 | 0.32 |
| | SED | – | 0.012 | | – | 0.01 | | – | 0.004 | | – | – | | 0.25[c] | 0.28[c] | | 0.025 | 0.023 | |
| | LSD | – | 0.025 | | – | 0.021 | | – | 0.008 | | – | – | | 0.52[c] | 0.58[c] | | 0.051 | 0.048 | |
| | *p* | 0.30 | 0.0002* | | 0.53 | 0.01* | | 0.20 | 0.0001* | | 0.73 | 0.08 | | 0.02* | 0.0002* | | 0.002* | <0.0001* | |

*Notes.* [a](1) averages over compaction treatments at different depths. [b](2) averages over sites at different depths. [c]SED and LSD values for $K_s$ are in $\log_{10}$ scale.
*$p$ < 0.05.

**TABLE 4** Compaction effects and interactions at different depths (10, 30 and 50 cm) and at both sites (Upper site and Lower site)

| Depth (cm) Site | Porosity ≥0.03 mm (m³ m⁻³) | | | Macropores ≥0.3 mm (m³ m⁻³) | | | Large mesopores 0.3–0.06 mm (m³ m⁻³) | | | Small mesopores 0.06–0.03 mm (m³ m⁻³) | | | $K_s$ (cm h⁻¹) | | | Bd (g cm⁻³) | | |
|---|---|---|---|---|---|---|---|---|---|---|---|---|---|---|---|---|---|---|
| | Control | Traffic | p | Control | Traffic | p | Control | Traffic | p | Control | Traffic | p | Control | Traffic | p | Control | Traffic | p |
| 10-Upper | 0.08 | 0.07 | 0.38 | 0.05 | 0.04 | 0.66 | 0.02 | 0.02 | 0.3 | 0.01 | 0.009 | 0.4 | 1.17 | 5.62 | 0.02* | 1.21 | 1.26 | 0.17 |
| 10-Lower | 0.03 | 0.008 | 0.10 | 0.01 | 0 | 0.24 | 0.01 | 0.01 | 0.58 | 0.005 | 0.006 | 0.63 | 0.26 | 0.93 | 0.05* | 1.27 | 1.35 | 0.05 |
| Interaction[a] | | | 0.58 | | | 0.6 | | | 0.66 | | | 0.35 | | | 0.7 | | | 0.55 |
| 30-Upper | 0.08 | 0.04 | 0.07 | 0.04 | 0.02 | 0.3 | 0.04 | 0.01 | 0.003* | 0.01 | 0.009 | 0.1 | 3.39 | 1.32 | 0.22 | 1.31 | 1.38 | 0.09 |
| 30-Lower | 0.01 | 0.01 | 0.82 | 0.001 | 0 | 0.52 | 0.01 | 0.01 | 0.84 | 0.003 | 0.008 | 0.04* | 0.71 | 0.07 | 0.007* | 1.37 | 1.46 | 0.08 |
| Interaction | | | 0.19 | | | 0.73 | | | 0.01* | | | 0.02* | | | 0.16 | | | 0.76 |
| 50-Upper | 0.12 | 0.12 | 0.9 | 0.06 | 0.06 | 0.97 | 0.04 | 0.05 | 0.76 | 0.01 | 0.01 | 0.34 | 6.92 | 19.5 | 0.29 | 1.2 | 1.2 | 0.82 |
| 50-Lower | 0.02 | 0.05 | 0.38 | 0.005 | 0.02 | 0.51 | 0.01 | 0.02 | 0.25 | 0.006 | 0.006 | 0.73 | 1.45 | 1.7 | 0.86 | 1.34 | 1.3 | 0.25 |
| Interaction | | | 0.58 | | | 0.62 | | | 0.53 | | | 0.65 | | | 0.5 | | | 0.49 |

*Notes.* [a]Interaction between site and compaction treatment; when it is significant, it means that compaction effects on sites had different trends. *$p < 0.05$.

of all their interactions, and random effects of blocks and plots. $K_s$ was $\log_{10}$-transformed before analysis. Standard errors of differences (SED) and least significant differences (LSD) are presented for effects that are significant at the 95% confidence level.

## 3 | RESULTS

### 3.1 | Penetrometer resistance and bulk density

The increase of penetration resistance below 25 cm depth (Figure 2) and significantly larger bulk densities found at 30 cm depth than at 10 and 50 cm (Table 2) suggest the presence of a compacted layer in the soil profile at this depth at both sites, even in the control treatment. Penetrometer resistance increased as a result of wheel traffic compaction between 5–10 cm ($p = 0.04$), 10–15 cm ($p = 0.052$) and 15–20 cm ($p = 0.05$) at the Lower site. In contrast, at the Upper site, penetrometer resistance was not affected by compaction in the topsoil, whereas the trafficked treatment tended to have greater penetrometer resistances in the subsoil at 40–50 cm depth but the differences were not statistically significant ($p = 0.09$ at 40–45 cm; $p = 0.08$ at 45–50 cm).

Averaging over treatments, the bulk density was greater at the Lower site than at the Upper site at all measured depths (Table 3), although these differences were only significant at 50 cm depth ($p = 0.0004$, Table 3). Averaged over sites, compaction resulted in significantly higher bulk densities at depths of 10 and 30 cm ($p = 0.03$ and 0.04, respectively, Table 3). The strongest effect of compaction was found at these two depths at the Lower site ($p = 0.05$ and 0.08,
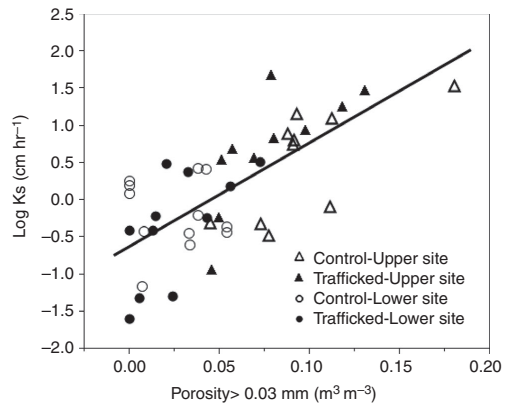


**FIGURE 3** Saturated hydraulic conductivity ($K_s$) as a function of porosity larger than 0.03 mm (corresponding to macropores, large mesopores and small mesopores). $\text{Log } K_s$ (cm hr⁻¹) = $-0.61 + 13.96 \times$ porosity (>0.03 mm in diameter)

respectively, see Table 4), in agreement with the measurements of penetrometer resistance (Figure 2).

## 3.2 | Pore size classes and saturated hydraulic conductivity

Significant differences were found in the pore size distribution between the sites, with much smaller values of macroporosity and mesoporosity at the Lower site at all three depths (see Table 3). Averaged over sites, the structural pore space (macropores and large mesopores >0.06 mm in diameter) was significantly smaller in the topsoil at 10 and 30 cm depth ($p = 0.02$ and 0.001, respectively) than in the subsoil at 50 cm depth (Table 3). The wheel trafficking treatment reduced the volume of large mesopores at 30 cm depth at the Upper site and increased the volume of small mesopores at 30 cm depth at the Lower site (Tables 3 and 4). No other significant effects of traffic compaction on the soil pore space were detected.

Averaged over sites, wheel trafficking significantly decreased saturated hydraulic conductivity ($K_s$) at 30 cm depth (Table 3). This was predominantly a result of an order of magnitude reduction in $K_s$ at the Lower site (Table 4). Trafficking followed by mouldboard ploughing significantly increased $K_s$ at 10 cm depth at both sites (Table 4). Combining data from both sites and all depths, Figure 3 shows that there is a clear relationship between mean values of $K_s$ and the volume of pores larger than 0.03 mm in diameter. Averaged over treatments, $K_s$ was significantly smaller at the Lower site than the Upper site at both 30 and 50 cm depth, which is in good agreement with the measurements of macro- and mesoporosity (Table 3, Figure 3).
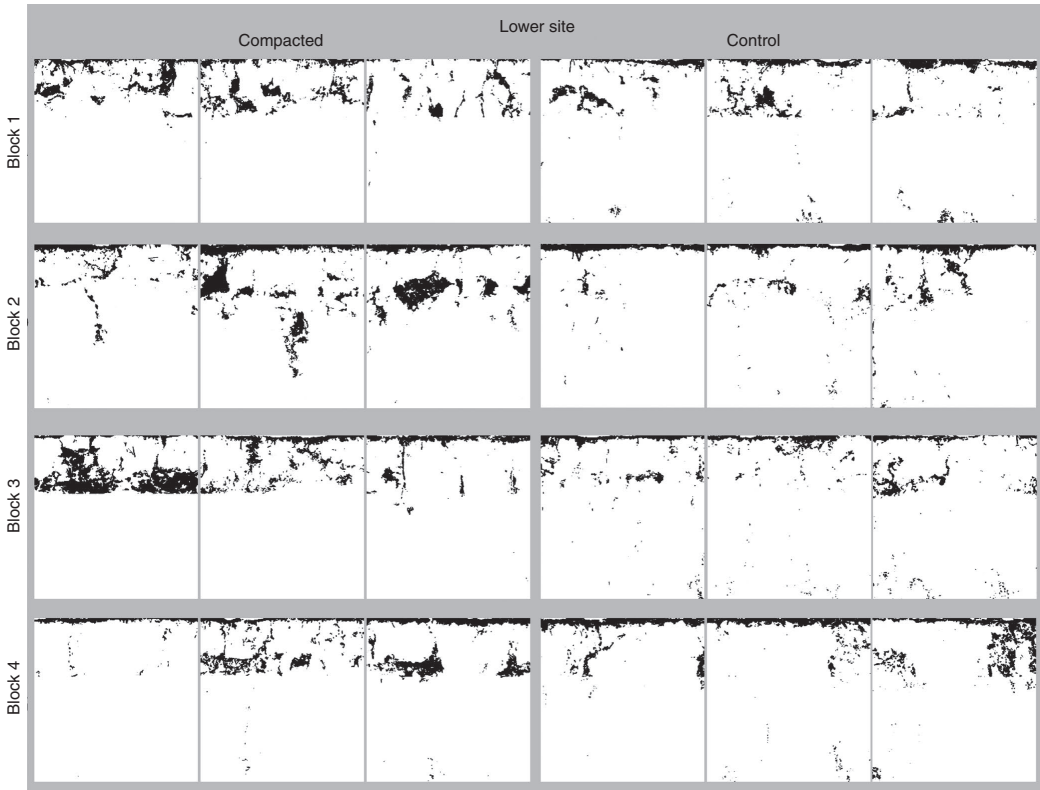
## 3.3 | Dye patterns

Figures 4 and 5 give a general overview of the dye patterns found in control and compacted plots at both sites. The dye
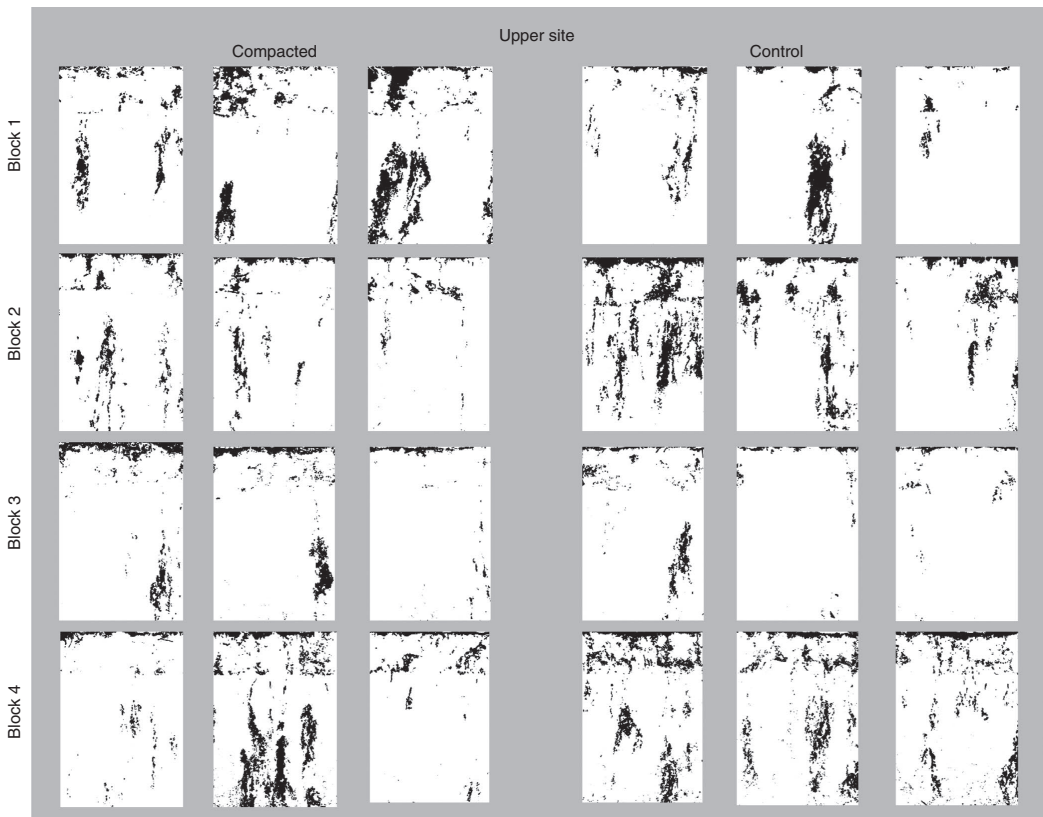


**FIGURE 4** An overview of the binary images obtained for the Upper site (photos were taken from 0 to 70 cm depth). The width of each photograph is ca.35 cm

**FIGURE 5** An overview of the binary images obtained for the Lower site (photos were taken from 0 to 100 cm depth). The width of each photograph is ca. 100 cm

tracing suggests the presence of a compacted layer at about 20–30 cm depth, which was also indicated by the penetrometer data and the measurements of soil physical properties. The presence of this compacted layer was very obvious at the Lower site, where the stained area was mostly concentrated above 30 cm depth. In contrast to the Upper site where up to 10 flow paths/m were found in the subsoil, very little staining was observed below 30 cm depth in both compacted and control plots at the Lower site (Figure 6). Compaction effects were associated with a smaller number of flow paths and a smaller dyed area in the whole profile of the trafficked treatment at the Upper site, although these differences were small compared with the very large variation between replicates (especially in the control treatment) so that the ranges overlapped (Figure 6). At the Lower site, wheel trafficking resulted in a clear increase in the dyed area in the topsoil at 5–25 cm depth. Although very little staining was found in the subsoil at the Lower site, some penetration of the dye to 70 cm depth was noted, but only in the control treatment (Figure 6).

## 4 | DISCUSSION

Effects of the wheeling treatment on soil physical or hydraulic properties and water flow patterns were more pronounced at the Lower site. The reasons for this are not clear, but one possibility is that the soil at the Upper site was drier at the time of wheeling and therefore more resistant to compaction, because it was under grass rather than cereal stubble. Significant effects of the traffic treatment on the structural pore space were found at 30 cm depth. Compaction effects were probably most pronounced at the 30 cm depth because on the one hand, soil stresses during compaction would have been much larger at 30 than at 50 cm depth (Keller, Ruiz, Arvidsson, Stettler, & Berli, 2016), and on the other hand, because ploughing could not help in accelerating recovery as it could at 10 cm depth because 30 cm is below tillage depth. We observed a decrease in the mesoporosity rather than macroporosity, perhaps partly because biopores survived after compaction (Blackwell, Green, & Mason, 1990;
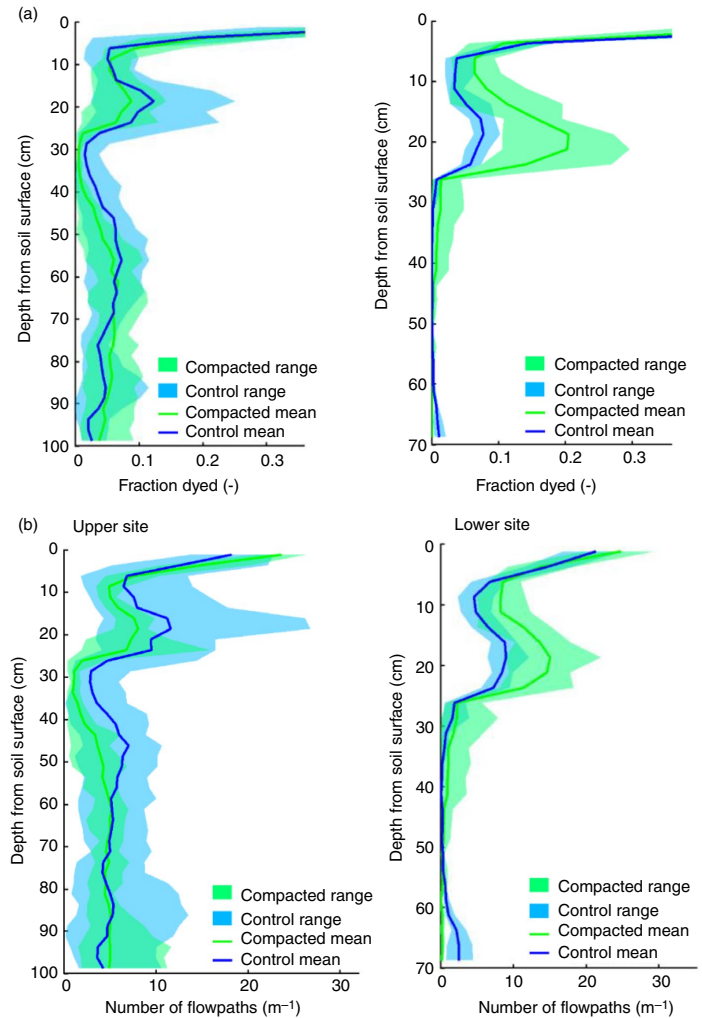
**FIGURE 6** Fraction dyed (a) and number of stained flow paths (b) at Upper and Lower sites in control and wheel trafficked treatments

Schäffer, Stauber, Mueller, Müller, & Schulin, 2008) and also because recovery induced by freeze–thaw, swell–shrink, macro-faunal activity and plant rooting (Dexter, 1991) may be slower or less efficient for these smaller pores. Larger $K_s$ values found at 10 cm depth at both sites in the traffic treatment may reflect a coarser structure and more continuous or larger shrinkage cracks after compaction and tillage of this fine-textured soil (Roger Estrade et al., 2004; Werner & Werner, 2001). It seems likely that not all of these cracks would have closed because of swelling during pre-saturation of the cores prior to $K_s$ measurement.

At the Lower site, ponding at the soil surface was observed during the dye-tracing experiments, especially in the trafficked plots, which supports the conclusion that infiltration and water flow were limited because of the presence of a compacted layer at plough depth characterized by a larger bulk density, as well as smaller macro- and mesoporosities and $K_s$ values. However, these ponding conditions at the Lower site did not induce any noticeable preferential transport of the dye solution deep into the subsoil. These observations are consistent with the results from an earlier study at this site reported by Mossadeghi-Björklund et al. (2016). For large columns sampled at 30–50 cm depth in the subsoil at the Lower site, they found almost no vertically continuous macroporosity on X-ray CT images and significantly slower solute transport was observed in breakthrough curve experiments compared with columns sampled from the Upper site. Our results for the Lower site contrast with

those of Kulli et al. (2003), who noted a drastic decrease in permeability of the topsoil caused by traffic, leading to local ponding and enhanced preferential flow into the subsoil of the compacted plots through continuous macropores that survived the compaction treatment. Consequently, they also reported more stained area in the subsoil as a result of compaction. However, they did not plough the soil between compaction and the dye-tracing experiment, as we did in our study. As in our study, Bogner, Mirzaei, Ruy, and Huwe (2013) also found large stained fractions at the base of the plough layer. They suggested that flow and transport processes above the plough pan were partly disconnected from those underneath because macropores were disrupted by tillage. However, in their study, preferential flow along cracks occurred on both compacted and control plots and the disconnected macropores below the tillage pan still functioned as preferential flow paths. This was not observed at the Lower site in our study, probably because there were too few continuous larger structural pores that could support preferential flow in the subsoil (Jarvis, Larsbo, & Koestel, 2017; Jarvis et al., 2016; Mossadeghi-Björklund et al., 2016). In contrast to the Lower site and despite the presence of a compacted layer at 25–30 cm depth, the Upper site has a much better developed structural porosity in the subsoil, which allowed preferential flow to reach to at least 1 m depth in both treatments.

## 5 | CONCLUSIONS

Contrasting effects of wheel traffic were found at the two sites as follows: one site under grass at the time of wheeling showed very little evidence of compaction induced by the wheel trafficking and consequently no treatment effects on water flow patterns. At the other site under cereal stubble, wheeling produced significant compaction in the plough layer, resulting in surface ponding during the dye-tracing experiments, with little evidence of preferential flow in the subsoil. We conclude that even quite small differences in initial conditions or soil and site properties may significantly influence the extent to which applied compaction stresses affect the connectivity of structural pore space in soil and consequently, water flow patterns.

## ORCID

*Mona Mossadeghi-Björklund* https://orcid.org/0000-0002-4624-5965

*Nicholas Jarvis* https://orcid.org/0000-0001-6725-6762

*Mats Larsbo* https://orcid.org/0000-0002-5162-2323

*Johannes Forkman* https://orcid.org/0000-0002-5796-0710

*Thomas Keller* https://orcid.org/0000-0002-9383-3209

## REFERENCES

Abramoff, D., Magalhaes, P. J., & Ram, S. J. (2004). Image processing with ImageJ. *Biophotonics International*, *11*, 36–42.

Alaoui, A., & Goetz, B. (2008). Dye tracer and infiltration experiments to investigate macropore flow. *Geoderma*, *144*, 279–286. https://doi.org/10.1016/j.geoderma.2007.11.020

Alaoui, A., Rogger, M., Peth, S., & Blöschl, G. (2018). Does soil compaction increase floods? A review. *Journal of Hydrology*, *557*, 631–642. https://doi.org/10.1016/j.jhydrol.2017.12.052

Blackwell, P. S., Green, T. W., & Mason, W. K. (1990). Responses of biopore channels from roots to compression by vertical stresses. *Soil Science Society of America Journal*, *54*, 1088–1091. https://doi.org/10.2136/sssaj1990.03615995005400040027x

Bogner, C., Mirzaei, M., Ruy, S., & Huwe, B. (2013). Microtopography, water storage and flow patterns in a fine-textured soil under agricultural use. *Hydrological Processes*, *27*, 1797–1806. https://doi.org/10.1002/hyp.9337

Dexter, A. R. (1991). Amelioration of soil by natural processes. *Soil and Tillage Research*, *20*, 87–100. https://doi.org/10.1016/0167-1987(91)90127-J

Etana, A., Larsbo, M., Keller, T., Arvidsson, J., Schjønning, P., Forkman, J., & Jarvis, N. (2013). Persistent subsoil compaction and its effects on preferential flow patterns in a loamy till soil. *Geoderma*, *192*, 430–436. https://doi.org/10.1016/j.geoderma.2012.08.015

Forrer, I., Papritz, A., Kasteel, R., Flühler, H., & Luca, D. (2000). Quantifying dye tracers in soil profiles by image processing. *European Journal of Soil Science*, *51*, 313–322. https://doi.org/10.1046/j.1365-2389.2000.00315.x

Håkansson, I., & Lipiec, J. (2000). A review of the usefulness of relative bulk density values in studies of soil structure and compaction. *Soil and Tillage Research*, *53*, 71–85. https://doi.org/10.1016/S0167-1987(99)00095-1

Jarvis, N. J. (2007). A review of non-equilibrium water flow and solute transport in soil macropores: Principles, controlling factors and consequences for water quality. *European Journal of Soil Sciences*, *58*, 523–546. https://doi.org/10.1111/j.1365-2389.2007.00915.x

Jarvis, N., Koestel, J., & Larsbo, M. (2016). Understanding preferential flow in the vadose zone: Recent advances and future prospects. *Vadose Zone Journal*, *15*(12), 11. https://doi.org/10.2136/vzj2016.09

Jarvis, N. J., Larsbo, M., & Koestel, J. (2017). Connectivity and percolation of structural pore networks in a cultivated silt loam soil quantified by X-ray tomography. *Geoderma*, *287*, 71–79. https://doi.org/10.1016/j.geoderma.2016.06.026

Keller, T., Ruiz, S., Arvidsson, J., Stettler, M., & Berli, M. (2016). Determining soil stress beneath a tire: Measurements and simulations. *Soil Science Society of America Journal*, *80*(3), 541–553. https://doi.org/10.2136/sssaj2015.07.0252

Kulli, B., Gysi, M., & Flühler, H. (2003). Visualizing soil compaction based on flow pattern analysis. *Soil and Tillage Research*, *70*, 29–40. https://doi.org/10.1016/S0167-1987(02)00121-6

Mossadeghi-Björklund, M., Arvidsson, J., Keller, T., Koestel, J., Lamandé, M., Larsbo, M., & Jarvis, N. (2016). Effects of subsoil compaction on hydraulic properties and preferential flow in a Swedish clay soil. *Soil Tillage Research*, *156*, 91–98. https://doi.org/10.1016/j.still.2015.09.013

Roger-Estrade, J., Richard, G., Caneill, J., Boizard, H., Coquet, Y., Defossez, P., & Manichon, H. (2004). Morphological characterization of soil structure in tilled fields: From a diagnosis method to the modelling of structural changes over time. *Soil and Tillage Research*, *79*, 33–49. https://doi.org/10.1016/j.still.2004.03.009

Rogger, M., Agnoletti, M., Alaoui, A., Bathurst, J. C., Bodner, G., Borga, M., … Blöschl, G. (2017). Land-use change impacts on floods – Challenges and opportunities for future research. *Water Resources Research*, *53*(7), 5209–5219. https://doi.org/10.1002/2017WR020723

Schäffer, B., Stauber, M., Mueller, T. L., Müller, R., & Schulin, R. (2008). Soil and macro-pores under uniaxial compression. I. Mechanical stability of repacked soil and deformation of different types of macro-pores. *Geoderma*, *146*, 183–191. https://doi.org/10.1016/j.geoderma.2008.05.019

Schindelin, J., Arganda-Carreras, I., Frise, E., Kaynig, V., Longair, M., Pietzsch, T., … Cardona, A. (2012). Fiji: An open-source platform for biological-image analysis. *Nature Methods*, *9*, 676–682. https://doi.org/10.1038/nmeth.2019

Werner, D., & Werner, B. (2001). Compaction and recovery of soil structure in a silty clay soil (Chernozem): Physical, computer tomographic and scanning electron microscopic investigations. *Journal of Plant Nutrition and Soil Science*, *164*, 79–90.

Soil compaction caused by agricultural machinery is a major threat to soil functions. Compaction modifies soil pore structure, but it has been unknown how this affects the occurrence of preferential flow. Preferential water flow can facilitate transport of nutrients and pollutants adversely affecting groundwater quality. This thesis examined the impact of compaction on soil hydraulic properties and preferential water flow based on laboratory and in situ measurements. It was found that preferential flow is strongest at intermediate compaction levels.

**Mona Mossadeghi Björklund**

Department of Soil and Environment, SLU

SLU generates knowledge for the sustainable use of biological natural resources. Research, education, extension, as well as environmental monitoring and assessment are used to achieve this goal.